Doctoral Dissertation

Influence of developers and underlayers on dissolution kinetics of photoresist films during development process for lithography

（リソグラフィ現像プロセスにおける
現像液と下地膜の影響）

Wang Jiahao

July 2025

Department of Applied Chemistry
Graduate School of Engineering
The University of Osaka

Preface

The investigation described in this thesis was performed under guidance of Professor Takahiro Kozawa at the SANKEN, Osaka University.

The objective of this research is to reveal the influence of developers and underlayers on the dissolution kinetics of photoresist films during development for the lithography. The components in the photoresist, developer condition and types of underlayer were varied, and their dissolution kinetics were clarified.

Contents

General Introduction

Development of lithography and photoresist

Semiconductor manufacturing in integrated circuits (ICs) is of importance in current life, underpinning the development and functionality of virtually every electronic device that we rely on today. From smartphones and computers to medical equipment, semiconductors enable advanced processing and connectivity. Nowadays, the demand for the ICs has been transferred from electronics to higher computation in artificial intelligence (AI) since the release of ChatGPT in 2022, opening a new advent for the AI era. As a result, an unstoppable demand for the ICs with high-performance chips has been a trend due to the continuous increase in the volume of data processing.

The density of ICs has increased in accordance with Moore's Law,[1)] and the scales are continuously increasing. Today, the large-scale integrated circuits with 10^{11} (100 billion) units of semiconductor elements in a single IC have been achieved. As a result, miniaturization and high integration in ICs are of importance, as well as the requirements for the matching manufacturing. For manufacturing, lithography technology plays an important role, and the schematic of lithography is shown in **Fig. 1**. Lithography is a process to transfer the pattern from the mask to the silicon wafer with light irradiation, including the spin-coating, development and etching. With the variation in the light sources, miniaturization in devices could be obtained.

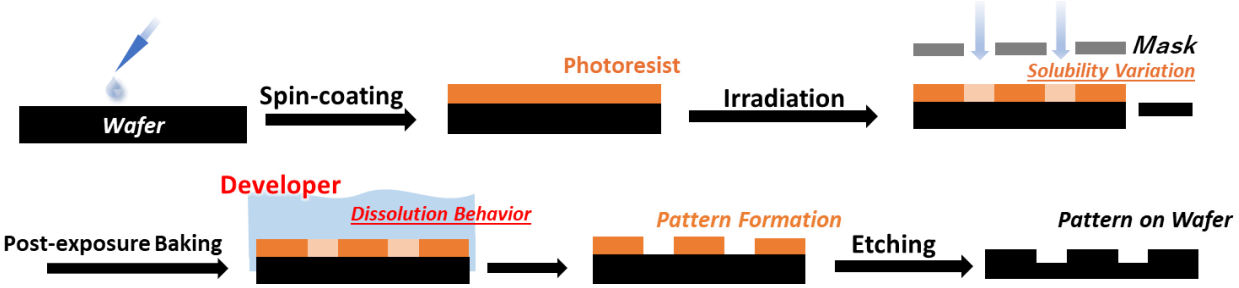

Fig. 1. The scheme for the lithography process.

The resolution, related to the critical dimension of as-formed pattern, has strong correlation with the wavelength of the light resource and the performance of the optical-exposure tool [numerical aperture (NA)], based on Rayleigh's formula in Eq. (1):

$$R = k_1 \frac{\lambda}{\mathrm{NA}}, \tag{1}$$

where R is the resolution, k_1 is the process constant, and λ is the wavelength. The wavelength of the exposure source is continuously shortened with the demand for the high-performance ICs.

The development of the lithography with the matching materials is shown in **Fig. 2**. The light source was improved from mercury g-line to i-line, KrF, and ArF excimer lasers. Extreme ultraviolet (EUV) lithography has been applied in the manufacturing since 2019.[2] In recent, an advancing exposure tool with 0.55 NA has been utilized to obtain the resolution below 8 nm half-pitch.[3] In addition, the exposure tool with higher NA, larger than 0.75, is under development and research as well.[4]

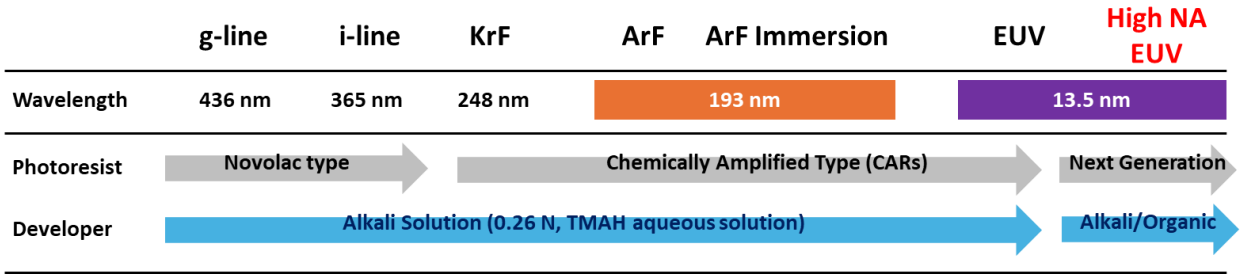

Fig. 2. The development of lithography and corresponding materials in different periods.

With the development of lithography, the materials are of importance as well. The chemically amplified photoresist (CAR) has been widely applied since KrF lithography, and still to be a competitive candidate in EUV lithography due to its property of high sensitivity. Three main components were contained in the CARs: the main polymer for the variation of solubility, the photoacid generator (PAG) as the reaction initiator, and the quencher to trap the proton to control the acid diffusion. Due to the high energy of EUV source, the reaction mechanism of EUV resists is related to the ionizing radiation chemistry,[5] as shown in **Fig. 3**.

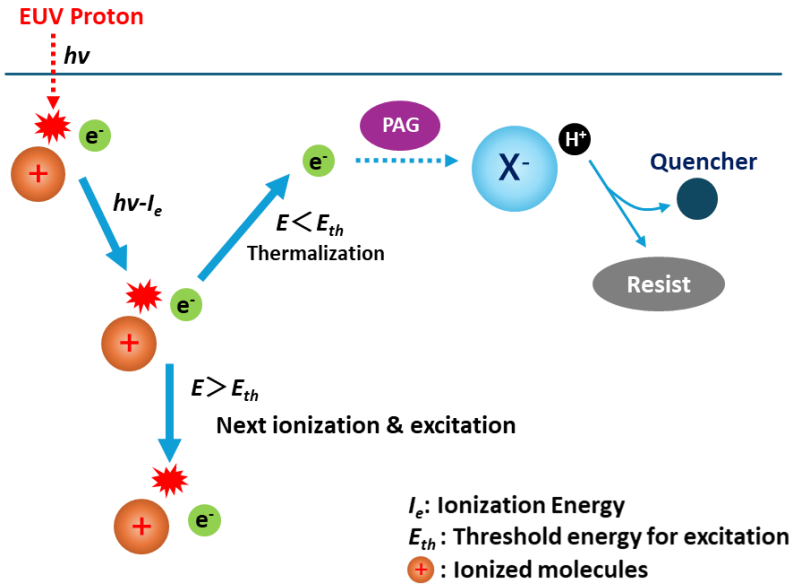

Fig. 3. Reaction mechanism in EUV resist.

The photoresist could absorb the EUV proton, and the photoelectron with excessive energy is emitted. Further ionization and electron excitation could be induced by the photoelectron. Due to the energy loss at excitation and ionization, the photoelectron and secondary electrons are finally thermalized. The proton is then generated by the oxidation of polymer molecules. The anion is generated by the reaction between the PAG and thermalized electrons. The generated acid initiates the reaction of photoresist polymer. During this period, some parts of protons are trapped by the quencher.

Pattern formation and stochastic defects

The pattern quality after the development is the most important. There are three factors in the trade-off relationship: sensitivity, resolution and line edge roughness (LER).[6] The adjustment of these relationships is one of the challenges in the lithography. In the EUV lithography, due to the low amount of photons available for patterning, namely, the limitation to the photon sensitivity, the stochastic defects such as the pinching and bridging due to the random fluctuation on the solubility of photoresist film are a serious concern.[7-9] In addition, with the improvement of the critical dimension, the photoresist film should be controlled within an optimal thickness, preventing the pattern collapse. As the reason for pattern collapse, the capillary force of the solvent is the main factor, as well as the ratio of height and the width of the pattern.[10-12] In general manufacturing, the underlayer was attached on the silicon wafer to enhance the adhesion between the substrate and photoresist film,[13-15] as well as the thinning in the thickness of photoresist film. However, the attachment of underlayer could complicate the interface effect between underlayer and resist film, and have a big influence on the pattern formation after the development.[14] As a result, the selection of the appropriate underlayer became an important issue.

The mechanism of the formation on stochastic defects in line-and-space pattern is shown in **Fig. 4**, according to the previous report.[16] The probability of pattern defects was thought to follow the Gaussian distribution, and the expectation was defined by $|N - N_{DT}| / \sigma$. The fluctuations of protected unit in photoresist existed in the center of lines and spaces, due to the stochastic distribution of PAG and quencher. In the center of spaces, the bridging would occur when the density of soluble units was lower than the dissolution threshold; around the center of lines, if the density of soluble units was higher than the dissolution threshold, the pattern would disappear, resulting in the pinching. In addition, the factor of pattern defect risk was related to the dissolution process as well, including the development and rinsing processes.

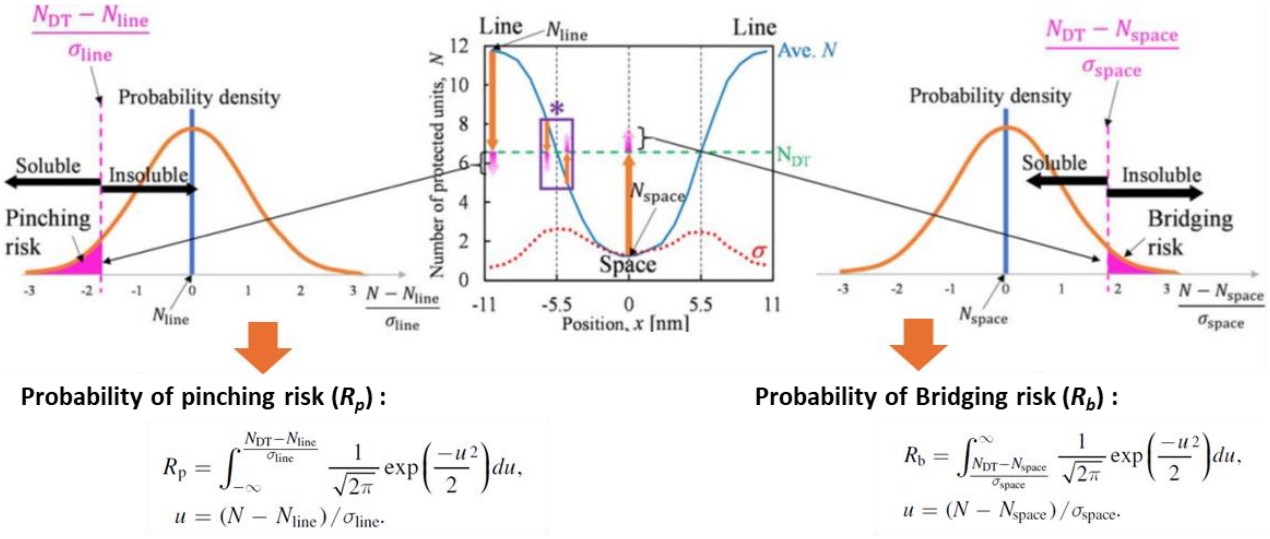

Fig. 4. Schematic of mechanism for stochastic defect generation.

Dissolution process and kinetics

As discussed in the previous section, the pattern defects are correlated to the development process. The dissolution kinetics of photoresist films during the development is of importance. According to the previous research, the discussion of dissolution kinetics was mainly divided into two parts: the dissolution type and dissolution rate.[17-21] With variation of developer, a dramatic variation existed in the dissolution of t-Boc PHS film, as well as the mechansim,[21] as shown in **Fig. 5**. The *t*-Boc PHS, the poly(4-hydroxystrene) (PHS) partially protected by the tert-butoxycarbonyl (t-Boc) group, was widely used as the CAR in the lithography. For the organic alkaline solution, such as the tetramethylammonium hydroxide (TMAH) aqueous solution, the PHS could be ionized by the OH^- in the solvent, and diffusion speed of dissociated polymer was rapid. As the macroscopic behavior, the swelling of photoresist film could be observed, while the thickness and existence time of film were varied with length of side chain in developer, as well as the developer concentration.[18,19] In the case of organic solution, due to the weak interaction between the solvent and resist film, the thick sol-gel layer would generally form. Even though the hydrogen bonding and instantaneous interaction was derived from the non-polar components, the dissociation force of polymer was still weaker than the coulomb force between the ions.

The existence of the underlayer could further complicate the dissolution kinetics as well. Due

to the interaction between the underlayer and resist film, the inter-mixing layer with several nanometers could exist, changing the properties of the resist films.[22] However, the detail on the dissolution kinetics of resist films with the underlayer remain unknown, and further research is in demand.

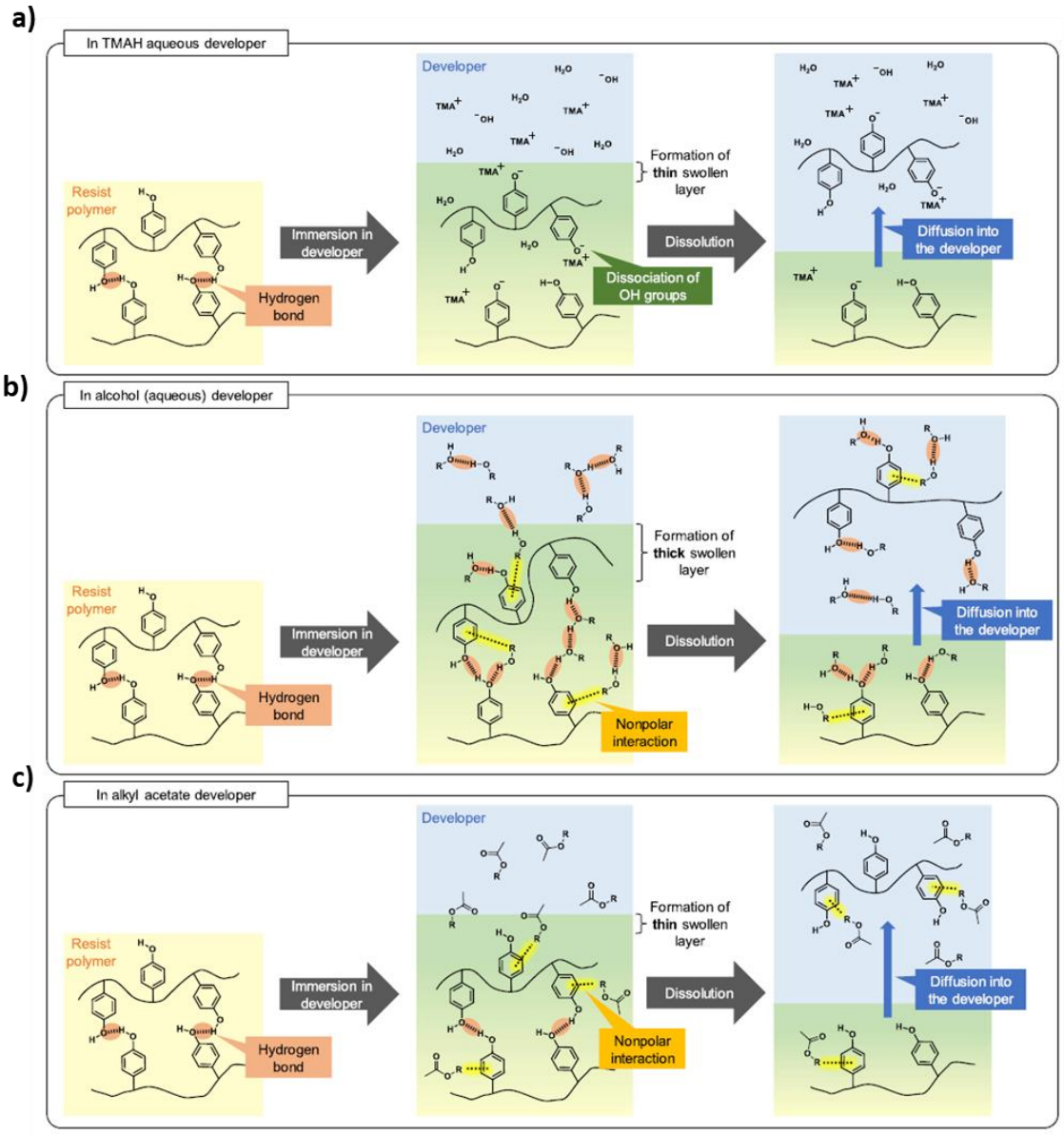

Fig. 5. Dissolution mechanism of t-Boc PHS film in (a) TMAH aqueous developer, (b) alcohol aqueous developer and (c) alkyl acetate developer.

Objectives

The interaction between the underlayer and photoresist film is complicated, and influence of underlayer on the dissolution kinetics of photoresist film is still unknown and remain for research.

In addition, the mechanism of dissolution varied with the type of developer and its concentration. In this study, I would like to reveal the relationships between the underlayer, photoresists, and developers during the development. The study could be divided into three sections:

In Chapter 1, the effect of the underlayer on the dissolution kinetics of photoresist films during the development was revealed. The *t*-Boc PHS was used as the photoresist, while the protection ratio was varied. The TMAH aqueous solutions with different concentrations were utilized as the developer. Nine types of underlayers with different surface free energy (SFE) were prepared in the experiments. The attenuation rate (α) was introduced to connect the relationship between the underlayer and dissolution kinetics of resist films.

In Chapter 2, the effect of underlayer on the deprotection process of photoresist films, containing the PAG and quencher, was revealed, as well as their dissolution kinetics affected by the deprotection process. Triphenylsulfonium nonaflate (TPS-nf) and triphenylsulfonium salicylate (TPS-sal) were used as a PAG and a photodecompsable quencher (PDQ), composing a three-component photoresist: *t*-Boc PHS/TPS-nf/TPS-sal. The standard TMAH aqueous solution (0.26 N) was used as a developer.

In Chapter 3, a new series of developers, the alkyl-trimethyl-ammonium hydroxide (A-TMAH) aqueous solutions, were utilized as the alternative of TMAH aqueous solution, and their dissolution kinetics of photoresist films were revealed. The *t*-Boc PHS with different protection ratio was used for the photoresist.

References

1) G. E. Moore, IEEE SSCS NEWSLETTER **38**, 8 (1965).
2) T. Itani, P. A. Gargini, P. P. Naulleau, and K. G. Ronse, Proc. SPIE **11147**, 1114701 (2019).
3) A. C. Gysen, C. W. Man, B. V. Meerten, H. V. Loo, E. V. Setten, S. Smith-Meerman, G. Yegen, D. D. Bruin, J. V. Schoot, R. Peeters, K. Bhattacharyya, G. Storms, and P Vanoppen, Proc. SPIE **PC13215**, PC132150 (2024).
4) G. Bottiglieri, P. Woltgens, R. v.d. Meer, S. Blok, B. Slachter, J. McNamara, M. v.d. Kerkhof, J. v. Schoot, M. Patra, J. T. Neumann, and H. Feldmann, Proc. SPIE **13424**, 1342404 (2025).
5) T. Kozawa and S. Tagawa, Jpn. J. Appl. Phys. **49**, 030001 (2010).
6) G. M. Gallatin, Proc. SPIE **5754**, 38 (2005).
7) P. D. Bisschop, J. Micro/Nanolith. MEMS MOEMS **16,** 041013 (2017).
8) P. D. Bisschop, E. Hendrickx, Proc. SPIE **10583**, 105831K (2018).

9) P. D. Bisschop, E. Hendrickx, Proc. SPIE **10957**, 109570E (2019).
10) T. Tanaka, M. Morigami, and N. Atoda, J. Appl. Phys. **32**, 6059 (1993).
11) H. Namatsu, K.Kurihara, M. Nagase, K. Iwadate, and K. Murase, Appl. Phys. Lett. **66**, 2655 (1995).
12) M. Harumoto, T. Motono, A. F. d. Santos, C. Mori, Y. Tanaka, H. Stokes, M. Asai, J. J. Santillan, T. Itani, and T. Kozawa. Jpn. J. Appl. Phys. **60**, SCCA03 (2021).
13) R. Sakamoto, B.-C. Ho, N. Fujitani, T. Endo, and R. Ohnishi, Proc. SPIE **7969**, 79692F (2011).
14) P. Vanelderen, N. Vandenbroeck, Y. Liang, V. V. Driessche, D. Guerrero, A. Chacko, D. D. Simone, and G. Vandenberghe, Proc. SPIE **11326**, 1132615 (2020).
15) R. Fallica, S. Chen, D. D. Simone, and H. S. Suh, J. Micro/Nanopatterning, Mater. Metrol. **21**, 34601 (2022).
16) K. Azumagawa and T. Kozawa, Jpn. J. Appl. Phys. **60**, SCCC02 (2021).
17) Y. T. Ito, K. Watanabe, T. Kozawa, K. Sakamoto, and M. Muramatsu. Jpn. J. Appl. Phys. **63**, 076506 (2024).
18) Y. T. Ito, H. Betsumiya, T. Kozawa, K. Sakamoto, and M. Muramatsu, Jpn. J. Appl. Phys. **61**, 066506 (2022).
19) H. Betsumiya, Y. T. Ito, T. Kozawa, K. Sakamoto, and M. Muramatsu, Jpn. J. Appl. Phys. **62**, 036503 (2023).
20) Y. Iwashige, Y. T. Ito, T. Kozawa, K. Sakamoto, and M. Muramatsu, Jpn. J. Appl. Phys. **62**, 036502 (2023).
21) Y. T. Ito, K. Watanabe, T. Kozawa, K. Sakamoto, and M. Muramatsu, Jpn. J. Appl. Phys. **63**, 076506 (2024).
22) S. W. Han, E. Byun, S.Kim, H. J. Lee, J. Yoon, Y. H. Kim, and S. Choi, J. Micro/Nanopattern. Mats. Metro. **23**, 044602 (2024).

Chapter 1 Relationship between surface free energy of underlayers and attenuation rate of poly(4-hydroxystyrene) partially protected by tert-butoxycarbonyl group in tetramethylammonium hydroxide aqueous solution

1-1. Introduction

In semiconductor devices, the size of transistors must be miniaturized to satisfy the request in higher integration and performance with less manufacturing cost. The extreme ultraviolet (EUV) radiation with the wavelength of 13.5 nm has been applied to the production line since 2019.[1)] To obtain the better resolution with 8 nm half-pitch, the numerical aperture (NA) of the optics with 0.55 NA will be utilized in the commercial manufacture in near future. However, the photoresist materials are still under investigation to find out the optimal conditions toward the optical resolution limit.[2)]

In the semiconductor lithography process for the mass production of semiconductor devices, chemically amplified resists (CARs)[3,4)] are potential next-generation photoresists for high NA EUV lithography to satisfy the sensitivity, resolution, and line width roughness (LWR).[5)] With the progress of miniaturization in the resolution, the thinning of photoresist film is an inevitable trend. The thinning of the films could restrain the pattern collapse during the development due to the surface tension of rinsing liquids.[6-8)] However, the thin film raised a big concern in the interfacial effects of polymer-type photoresist as well.[9,10)] It is reported that the glass transition temperature of interfacial layer differs from that of bulk layer,[11)] as well as the expansivity and viscosity of polymer.[12,13)] The initial thickness of film also has an influence on the dissolution rate and dissolution behavior of interfacial layer.[14)] As a result, the thinning of film intensifies the interfacial effects, resulting in a big difference in the chemical condition and dissolution kinetics near interfacial layer.

To improve the photoresist performance, the underlayer is generally attached between the substrate and photoresist.[15)] According to the previous research, the underlayer could suppress the pattern collapse and improve the performance of photoresist by decreasing the LWR.[16)] However, the adhesion of underlayer would further complicate the condition of the interfacial layer of photoresist. The interaction between underlayer and photoresist is vital to clarify the condition of interfacial layer. The surface free energy of underlayer, the polar and dispersion components, was an important key to determine the interaction between two materials.[17,18)] In the previous report, our group successfully connected the relationship between underlayer and photoresist during the dissolution process that the attenuation rates of photoresist films varied with the surface free

energy of underlayers.[19] In addition, the dissolution kinetics of photoresists was affected by the types and concentration of developer as well.[20,21] However, the details of the interaction between underlayer and photoresist is still unclear. It is necessary to ulteriorly reveal the relationship between the dissolution dynamics of photoresist films and the surface free energy of underlayers in different conditions.

In this chapter, the dissolution dynamics of photoresist with different underlayers in developers with different concentrations were observed and the relationship between the attenuation rate of developer viscosity and the surface free energy of photoresist films was discussed. The t-Boc PHS was prepared as the photoresist. Tetramethylammonium hydroxide (TMAH) aqueous solution was utilized as a developer, and its concentration was varied. The quartz crystal microbalance (QCM) method was introduced to investigate the dissolution dynamics.

1-2. Experiments

PHS (Mw ~11000) and propylene glycol monomethyl ether acetate (PGMEA) were purchased from Sigma-Aldrich. The hydroxyl group of PHS was partially protected by the *t*-Boc groups. The protection ratios of PHS were 10 and 30%. The PHS partially protected with the protection ratios of 0, 10, and 30% was named as 0, 10, and 30% *t*-Boc PHS, respectively, for simplicity. The TMAH aqueous developer NMD-3 (2.38 wt%, 0.26 M) was purchased from Tokyo Ohka Kogyo, and diluted by the water to prepare 1.43 and 0.95 wt% aqueous solution (0.26 and 0.16 M, respectively). The molecular structures of photoresist and TMAH are shown in **Fig. 1-1**. The underlayer solutions were supplied by Nissan Chemical Corp. The chemical structures of end groups and the surface free energies of underlayers are shown in **Fig. 1-2**.

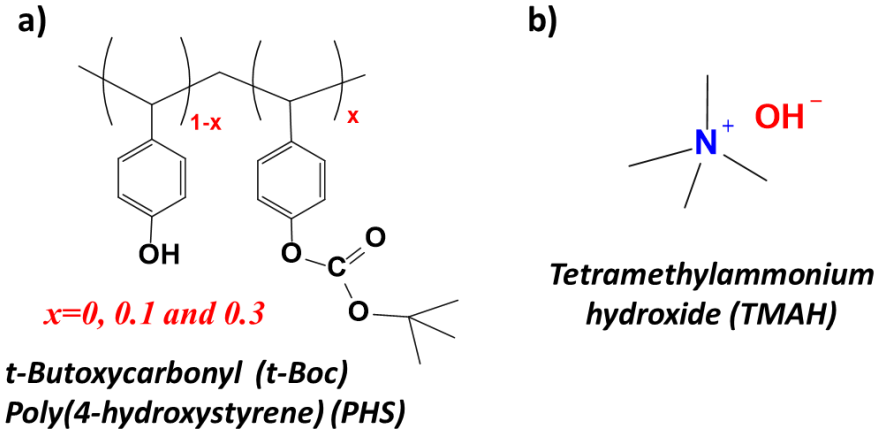

Fig. 1-1. The molecular structures of (a) *t*-Boc PHS and (b) TMAH.

	None	NCX11085	NCX11086	NCX11087	NCX11088	NCX11089	NCX11090	NCX11286	NCX11287	NCX11288
	Au (Aurum)		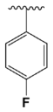	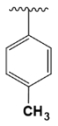	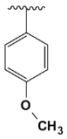	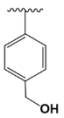	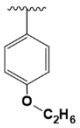	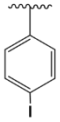	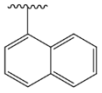	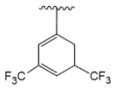
Polar	2.5	9.9	8.5	7.7	10.8	16.9	4.3	6.2	6.8	5.2
Dispersion	36.9	35.4	32.7	34.2	35.1	34.4	33.1	42.8	39.1	19.3
Ratio	0.067	0.280	0.260	0.389	0.308	0.491	0.130	0.145	0.174	0.269

**The units of polar and dispersion component are mJ/m^2.*

Fig. 1-2. The chemical structures of end groups and the surface free energies of underlayers. NCX11086 and NCX11286 are marked in red color due to the halogen end groups.

The underlayers were spin-coated on QCM substrates to obtain films with approximately 40 nm thickness and prebaked at 205 °C for 60 s. The *t*-Boc PHS powder was dissolved in the PGMEA and spin-coated on the underlayers or directly on the QCM substrates to obtain the films with approximately 200 nm thickness, followed by the pre-baking at 90 °C for 90 s. The as-prepared samples were developed in the TMAH aqueous developers, and the dissolution kinetics was observed by the QCM-based development analyzer (Litho Tech Japan RDA-Qz3).[22] The film thicknesses before and after development were measured using an ellipsometer (Meiwafosis FS-1).

The QCM method is rapid, real-time, and effective to detect the dissolution dynamics of films during the development. The QCM substrate is composed of the crystal quartz and Au electrodes, where the quartz is sandwiched between the electrodes. Due to the piezoelectric properties of the quartz crystal, the weight change and viscoelastic property of films could be observed from the frequency (Δf) and impedance (Z).[23,24]

The variation in the frequency corresponds to the swelling and dissolution of polymer films. According to the previous study, the change in frequency can be converted to the weight change on the QCM substrate in accordance with Sauerbrey's equation:[25]

$$\Delta f = -\frac{2{f_0}^2}{A\sqrt{\rho_q \mu_q}}\Delta m, \tag{1}$$

where Δf, f_0, Δm, A, ρ_q, and μ_q are the frequency change, the resonant frequency of the unloaded QCM substrate, the mass change of the material on the substrate, the piezoelectrically active crystal area, the density of quartz, and the shear modulus of the quartz used as the AT-cut crystal, respectively. The impedance (Z) during the development is related to the viscoelasticity of the film and the viscosity of the contacting liquid on the QCM substrate. The impedance change was

attributed to the power dissipation due to the propagation of damped shear wave into the liquid around the oscillating QCM substrate surface.[26)]

Attenuation rate of impedance (α) is a constant related to the propagation of dissolved polymer film into the solution during the development. In the previous study, the relationship between the decay of impedance (Z) and attenuation rate was reported to be followed by the following equation:[19,20)]

$$Z = \frac{z_0}{(t-t_0)^{\alpha}} + b, \tag{2}$$

where the Z_0, t, t_0, α, and b are the constant, the development time (s), the reference time (s), the attenuation rate, and the baseline, respectively.

1-3. Results and Discussion

The films of *t*-Boc PHS with and without underlayers were developed in TMAH aqueous solutions, and the dissolution kinetics were observed by the QCM analyzer. Due to the rapid dissolution of 0% *t*-Boc PHS films, the dissolution kinetics in developer with high (standard) TMAH concentration could not be detected. Instead, 0.95 wt% TMAH aqueous solution (0.1 M) was applied. In the case of 10% and 30% *t*-Boc PHS films, 2.38 wt% and 1.43 wt% TMAH aqueous solutions were utilized as the developer, respectively. The attenuation rate (α) was obtained by the least square fitting, based on the relationship described in the experiment section. The dissolution kinetics of 10% *t*-Boc PHS films in 1.43wt% TMAH aqueous solution is shown in **Fig. 1-3**, as well as an example of fitting curve of impedance variation.

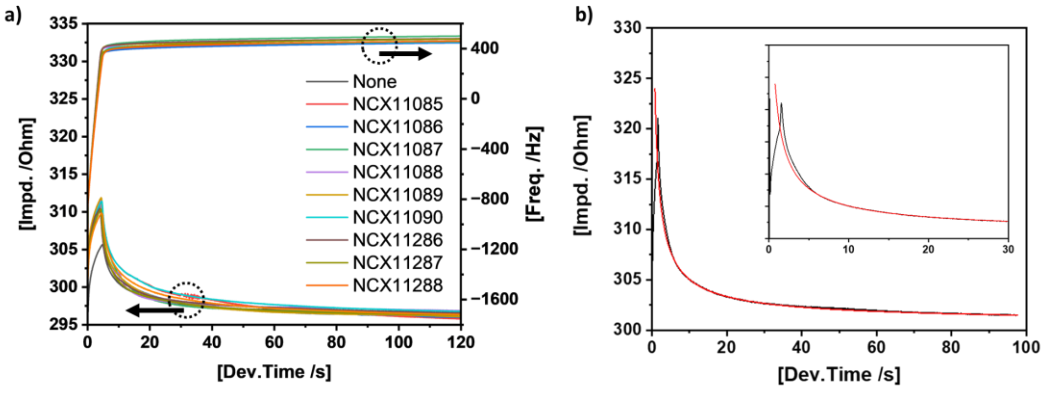

Fig. 1-3. (a) The dissolution kinetics of 10% *t*-Boc PHS films with and without underlayers in 1.43 wt% TMAH aqueous solutions. (b) The least square fitting of 30% *t*-Boc PHS films without the underlayer in the 2.38 wt% TMAH aqueous solution. The red line is the fitting curve. The inset in (b) is an enlarged figure in terms of development time (30 s).

Table 1-1. Attenuation rates of *t*-Boc PHS films in TMAH aqueous solutions with different TMAH concentrations.

t-Boc (%)	TMAH (wt%)	Underlayer				
		None	NCX11085	NCX11086	NCX11087	NCX11088
0	0.95	0.59±0.18	0.72±0.24	0.84±0.33	0.40±0.13	0.60±0.14
10	1.43	0.69±0.18	0.56±0.29	0.60±0.10	0.67±0.21	0.42±0.30
	2.38	0.80±0.22	0.86±0.27	0.82±0.21	0.76±0.15	0.88±0.18
30	1.43	0.85±0.38	0.67±0.21	0.52±0.12	0.62±0.16	0.61±0.26
	2.38	0.75±0.20	0.70±0.14	0.83±0.16	0.72±0.25	0.86±0.29

t-Boc (%)	TMAH (wt%)	Underlayer				
		NCX11089	NCX11090	NCX11286	NCX11287	NCX11288
0	0.95	0.70±0.20	0.65±0.20	0.52±0.13	0.33±0.18	0.50±0.13
10	1.43	0.86±0.19	0.56±0.19	0.61±0.28	0.80±0.10	0.66±0.11
	2.38	1.00±0.14	0.96±0.19	0.68±0.25	0.84±0.30	0.66±0.18
30	1.43	0.50±0.23	0.63±0.18	0.68±0.24	0.64±0.15	0.64±0.15
	2.38	0.84±0.42	0.85±0.24	1.00±0.31	0.66±0.21	0.68±0.29

All the attenuation rates (α) of *t*-Boc PHS films in the developers with the different TMAH concentrations are shown in **Table 1-1**. In the previous research, the relationship between attenuation rate and surface free energy was unclear when the dispersion component of underlayer was similar.[19] As shown in **Fig. 1-4**, no obvious relationship was discovered between α and dispersion component similarly to the case of polar component, even though the dispersion component of underlayer was controlled in the similar scale to polar component; instead, an apparent tendency was found out between the α and the ratio of polar to dispersion components (component ratio). As indicated in **Fig. 1-5**, α was first decreased and then increased with the component ratio and an inflection point with the lowest value existed. However, the underlayer with halogen groups, marked as red dots in figures, showed irregular values in the attenuation rates for all types of *t*-Boc PHS films. Such a characteristic behavior was speculated as the effect of halogen bonding.[27,28] The existence of halogen end groups would result in the anomalous molecular arrangements of underlayer and further complicate the interface between the underlayer and *t*-Boc PHS films. Thus, the results of underlayer with halogen groups (NCX11086 and 286) were excluded in the following discussion about the trend in the dependence of α on the surface free energy.

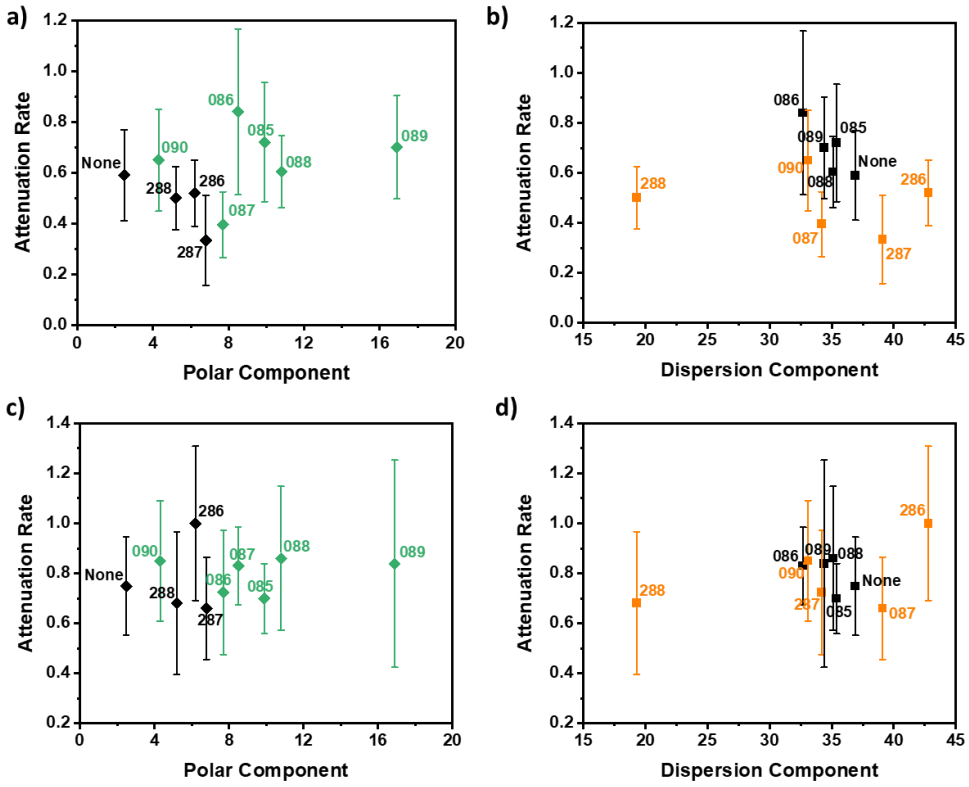

Fig. 1-4. The relationship between the attenuation rate (α) of *t*-Boc PHS films and the surface free energy of underlayers. (a), (b) Relationships between α of 0% *t*-Boc PHS films in 0.95 wt% TMAH concentration and polar and dispersion components. (c), (d) Relationship between α of 30% *t*-Boc PHS films in 2.38 wt% TMAH concentration and polar and dispersion components. The green dots indicate the underlayers with a similar dispersion component value in (a) and (c), while the orange dots were those with a similar polar component value in (b) and (d).

Besides, the inflection point of the attenuation rate was varied with the protection ratio of *t*-Boc PHS films, as shown in **Figs. 1-5(b)** and **1-5(c)**. In the case of 2.38 wt% TMAH aqueous solution, when the protection ratio was increased from 10% to 30%, the inflection point was shifted leftward from approximately 0.28 (around NCX11288) to approximately 0.25 (between NCX11087 and 288). Such a shift corresponds to the variation of surface free energy in the *t*-Boc PHS film. The polar component of the surface free energy of *t*-Boc PHS films decreased with the increase of protection ratio, while the dispersion component slightly increased.[21] Thus, the component ratio of *t*-Boc PHS films decreases with the protection ratio.

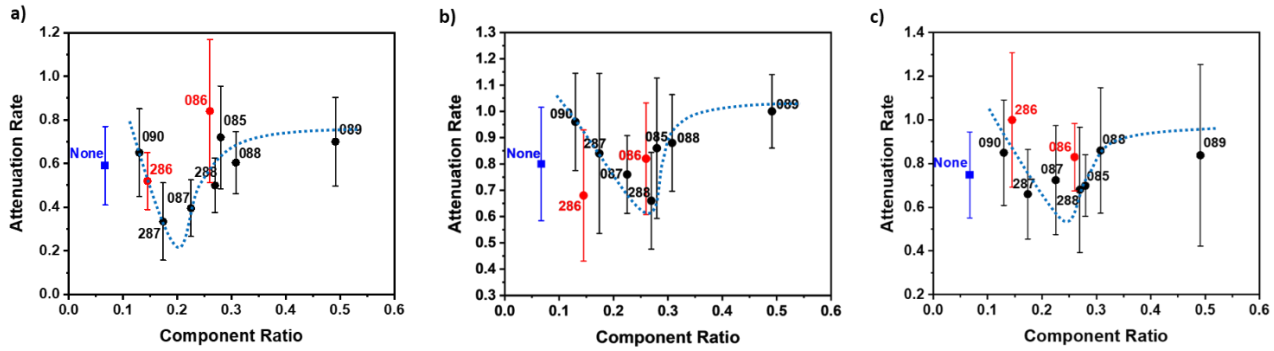

Fig. 1-5. The relationship between the attenuation rate (α) and the ratio of polar to dispersion components: (a) 0% *t*-Boc PHS films in 0.95 wt% TMAH developer, (b) 10% *t*-Boc PHS and (c) 30% *t*-Boc PHS films in 2.38 wt% TMAH developer. The red dots indicate the underlayers with halogen groups, while the blue dots indicate the datum without underlayer. The dash line with blue color is the probable tendency between α and the ratio.

The influence of TMAH concentration on the relationship between attenuation rate and component ratio was revealed in **Fig. 1-6**. The inflection point was shifted rightward from the position around NCX11288 to that between NCX11088 and NCX11089 in the case of 10% *t*-Boc PHS films when the TMAH concentration decreased from 2.38 to 1.43 wt% **[Figs. 1-5(b)** and **1-6(a)]**; however, the inflection point was not distinct in the case of 30% *t*-Boc PHS films in 1.43 wt% TMAH aqueous solution, due to the lack of underlayers between NCX11088 and 089 [**Figs. 1-5(c)** and **1-6(b)**]. As a result, the inflection point might be on the right of NCX11089 or between NCX11088 and 089. On the other hand, the dilution of the developer also decreased the difference of α among the underlayers as well. In the case of 10% *t*-Boc PHS films, the gradient of the tendency in 1.43 wt% TMAH developer was not as strong as that in 2.38 wt% TMAH developer [**Figs. 1-5(b)** and **1-6(a)**]; the similar phenomenon occurred in 30% *t*-Boc PHS films in 1.43 wt% TMAH developer that α was almost the same within the range of component ratio from 0.1 to 0.3 and the value was generally smaller than that in 2.38 wt% TMAH developer [**Figs. 1-5(c)** and **1-6(b)**].

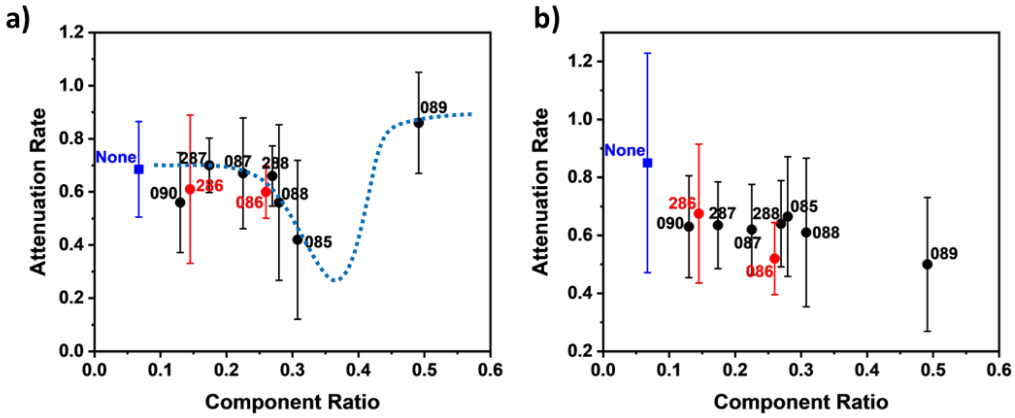

Fig. 1-6. The influence of TMAH concentration on the relationship between attenuation rate and component ratio: (a) the attenuation rate of 10% *t*-Boc PHS films in 1.43 wt% TMAH developer and (b) that of 30% *t*-Boc PHS films in 1.43 wt% TMAH developer. The dash line with blue color is the probable tendency between α and the ratio.

The relationship between underlayers, photoresists, and developers were revealed in this study, and quantified by using the attenuation rate (α) of *t*-Boc PHS films, the surface free energy (the ratio of polar to dispersion components) of underlayers, and the TMAH concentration of aqueous developer. α somehow described the rapid or slow diffusion of dissolved polymer (sol states) into developers; the surface free energy was utilized to indicate the weak or strong interaction between the photoresist and underlayers; the influence of TMAH concentration was expressed by the effect on α and the shift of inflection point. The inflection point played an important role in the relationship between α and surface free energy. In the position of inflection point, due to the strong interaction between underlayer and photoresist, the polymer film slowly dissolved and diffused in the developer; on the contrary, the weak interaction resulted in the fast dissolution and diffusion of polymer, showing the high value in α.

The discovery was interesting in the protection ratio of *t*-Boc PHS and α as well. The inflection point of component ratio was shifted rightward by increasing the protection ratio of *t*-Boc PHS films. Such a phenomenon was reversed to the rule that the polar to dispersion components should be similar to obtaining the strong interaction between underlayer and photoresist.

The above two phenomena were supposed to be useful to the material and process design. On the other hand, with a certain underlayer with definite component ratio, α of *t*-Boc PHS films with different protection ratios could be obtained. In theory, the gradient of protection ratio in the soluble part of the photoresist is generated by the exposure to light and the subsequent chemical

reactions.[29-31] Therefore, the interaction between photoresist and underlayer depends on the horizontal position on the underlayer. Furthermore, the pH of developer changes by the neutralization of TMAH with the acidic units of resist polymers such as phenolic hydroxyl and carboxylic acids. For the ultrafine patterning, these complicated dissolution dynamics near the underlayer should be controlled. Actually, there remain some problems in this study such as the absence of photoacid generator (PAG) and photo-decomposable quencher (PDQ). Although the real application to material and process design requires further detailed investigation, this study successfully took a first step towards it.

1-4. Conclusion

The relationship between attenuation rate (α) of *t*-Boc PHS films and the surface free energy of the underlayer in TMAH aqueous solution was revealed in this study. The α was related to the ratio of polar to dispersion components of the underlayer, rather than the single component. α was first increased and then decreased with the component ratio, and the inflection point with the lowest α existed. The protection ratio of *t*-Boc PHS and the TMAH concentration would affect the position of inflection point. With the increased protection ratio in *t*-Boc PHS, the inflection point shifted rightward to the lower component ratio, while the dilution of developer would result in the rightward shift of the inflection point and the decrease of α. Such consequence had the potential to be applied to other dissolution systems of underlayers, photoresists, and developers.

References

1) T. Itani, P. A. Gargini, P. P. Naulleau, and K. G. Ronse, Proc. SPIE **11147**, 1114701 (2019).
2) P. Gräupner, P. Kürz, J. Stoeldraijer, and J. Van Schoot, Proc. SPIE **11854**, 118540F (2021).
3) H. Ito and C. G. Willson, Polym. Eng. Sci. **23**, 1012 (1983).
4) H. Ito, Microlithography/Molecular Imprinting (Springer, Heidelberg, 2005) Advances in Polymer Science Series, Vol. 172, p. 37.
5) I. Mochi, K. Garrido Olvera, M. Meeuwissen, O. Yildirim, R. Custers, R. Hoefnagels, G. Rispens, M. Vockenhuber, Y. Ekinci, and Z. Tasdemir, Proc. SPIE **10583**, 105831W (2018).
6) M. Harumoto, T. Motono, A. F. Dos Santos, C. Mori, Y. Tanaka, H. Stokes, M. Asai, J. J. Santillan, T. Itani, and T. Kozawa, Jpn. J. Appl. Phys. **60**, SCCA03 (2021).
7) S. F. Chini and A. Amirfazli, Langmuir **26**, 13707 (2010).
8) T. Tanaka, M. Morigami, and N. Atoda, Jpn. J. Appl. Phys. **32**, 6059 (1993).

9) T. Kozawa and T. Tamura, Jpn. J. Appl. Phys. **60**, 086503 (2021).
10) L. Singh, P. J. Ludovice, and C. L. Henderson, Proc. SPIE **5039**, 1008 (2003).
11) R. A. L. Jones, Curr. Opin. Colloid Interface Sci. **4**, 153 (1999).
12) Q. Xu, N. Zhu, H. Fang, X. Wang, R. D. Priestley, and B. Zuo, ACS Macro. Lett. **10**, 1 (2021).
13) B. Zuo, F. Wang, Z. Hao, H. He, S. Zhang, R. D. Priestley, and X. Wang, Macromolecules **52**, 3753 (2019).
14) N. Maeda, A. Konda, K. Okamoto, T. Kozawa, and T. Tamura, Jpn. J. Appl. Phys. **59**, 086501 (2020).
15) M. Padmanaban, J. Cho, T. Kudo, S. Mullen, H. Yao, G. Noya, Y. Matsuura, Y. Ide, J. Li, and G. Pawlowski, Proc. SPIE **8682**, 868215 (2013).
16) R. Sakamoto, B.-C. Ho, N. Fujitani, T. Endo, and R. Ohnishi, Proc. SPIE **7969**, 79692F (2011).
17) R. Fallica, S. Chen, D. De Simone, and H. S. Suh, J. Micro/Nanopatterning, Materials and Metrology **21**, 34601 (2022).
18) P. Vanelderen, N. Vandenbroeck, Y. Liang, V. Van Driessche, D. Guerrero, A. Chacko, D. De Simone, and G. Vandenberghe, Proc. SPIE **11326**, 1132615 (2020).
19) T. Otsuka, Y. Jin, N. Tanaka, and T. Kozawa, Jpn. J. Appl. Phys. **61**, 056503 (2022).
20) Y. T. Ito, H. Betsumiya, T. Kozawa, K. Sakamoto, and M. Muramatsu, Jpn. J. Appl. Phys. **61**, 066506 (2022).
21) H. Betsumiya, Y. T. Ito, T. Kozawa, K. Sakamoto, and M. Muramatsu, Jpn. J. Appl. Phys. **62**, 036503 (2023).
22) A. Sekiguchi, J. Photopolymer Sci. Technol. **26**, 479 (2013).
23) S. W. Lee, W. D. Hinsberg, and K. K. Kanazawa, Anal. Chem. **74**, 125 (2002).
24) K. K. Kanazawa, Faraday Discuss. **107**, 77 (1997).
25) G. Sauerbrey, Z. Physik **155**, 206 (1959).
26) M. V. Voinova, M. Rodahl, M. Jonson, and B. Kasemo, Phys. Scr. **59**, 391 (1999).
27) G. Cavallo, P. Metrangolo, R. Milani, T. Pilati, A. Priimagi, G. Resnati, and G. Terraneo, Chem. Rev. **116**, 2478(2016).
28) J. Teyssandier, K. S. Mali, and S. De Feyter, Chemistry Open **9**, 225 (2020).
29) T. Kozawa, Jpn. J. Appl. Phys. **61**, 106502 (2022).
30) T. Kozawa, Jpn. J. Appl. Phys. **62**, 016509 (2023).
31) T. Kozawa, Jpn. J. Appl. Phys. **62**, 076501 (2023).

Chapter 2 Influence of underlayer on development of chemically amplified photoresist films in tetramethylammonium hydroxide aqueous developer

2-1. Introduction

The demand for integrated circuits (ICs) is growing rapidly owing to the development of artificial intelligence, resulting in higher demands on the performance, integration level, and production-cost reduction of transistors. To satisfy the above requirements, extreme ultraviolet (EUV) lithography has been applied in semiconductor manufacturing since 2019.[1)] Recently an optical-exposure tool with a numerical aperture (NA) of 0.55, called a high-NA tool, was utilized in EUV lithography to obtain a half-pitch resolution below 8 nm.[2)] Such equipment could further increase the production scale at a lower cost, through dose reduction. However, a series of problems remains to be addressed in the current stage, such as the depth of focus, image contrast, throughput, and well-matching mask.[3-7)]

The lack of an optimal photoresist is a serious problem in the high-volume manufacturing of semiconductors. Chemically amplified photoresists (CARs) are potential candidates for high-NA EUV lithography. Generally, CARs contain three components: a main-body polymer, photoacid generator (PAG), and photodecomposable quencher (PDQ). Photoprotons are generated in CARs with the assistance of PAG,[8)] activating the reaction of the main-body polymer to change the solubility during post-exposure baking (PEB). The PDQ absorbs the protons to restrain their propagation and reaction within the polymer matrix. Owing to the presence of PAG and PDQ, even though CARs exhibit high sensitivity, the stochastic effect of the heterogeneous distribution of photons can cause pattern defects after development.[9-13)] The effect of insufficient or over-sufficient absorption of photons in certain areas can be amplified by the chemical reaction during PEB, resulting in “bridge” and “pinch” defects in the pattern. In conclusion, a suitable failure-free critical-dimension window must be established for photoresists.

To improve the performance and pattern collapse of the photoresist during development because of the surface tension of the rinsing liquid, an underlayer is generally used between the substrate and photoresist.[14-17)] However, the addition of an underlayer can complicate the interactions at the interface between underlayer and photoresist. The interactions between the underlayer and photoresist can influence the dissolution behavior during the development. The surface free-energy (SFE) of the underlayer and photoresist film has a great influence on the pattern formation in the photoresist.[18-20)] It was reported that the ratio of the polar to dispersion component was a decisive factor in the dissolution behavior of PHS in a tetramethylammonium

hydroxide (TMAH) aqueous solution.[20] However, the dissolution behavior of complex polymer films including PAG and PDQ along with the underlayer, was not clear, and the effects of the additive on the photoresist remained unknown. Therefore, revealing the influence of PAG and PDQ on the photoresist during baking and the dissolution behavior of the photoresist with the underlayer during development is important. In practice, the multicomponent photoresist used in this study is closer to the real material used in the high-volume production lines of semiconductor devices than the PHS films used in the previous study. As a result, the research of multicomponent photoresist was believed to play a guiding role in real lithography.

In this chapter, the dissolution dynamics of photoresists containing PAG and PDQ are observed with different underlayers in the developer. The influence of PAG and PDQ on the photoresist after exposure is also revealed. The t-Boc PHS is prepared as a photoresist. An aqueous solution of TMAH is used as the developer. The quartz crystal microbalance (QCM) method is used to investigate dissolution dynamics.

2-2. Experiments

The *t*-Boc PHS with a protection ratio of 70 mol% was purchased from NARD. Propylene glycol monomethyl ether acetate (PGMEA) was purchased from Sigma-Aldrich. Powders of triphenylsulfonium nonaflate (TPS-nf) and triphenylsulfonium salicylate (TPS-sal) were purchased from Midori Kagaku Co., Ltd. and were used as the PAG and PDQ, respectively. *t*-Boc PHS, TPS-nf, and TPS-sal were dissolved in PGMEA to prepare the photoresist solution, where the weight ratio of *t*-BOC PHS, TPS-nf, TPS-sal, and the solvent was 1:0.1:0.05:9. The aqueous TMAH developer NMD-3 (2.38 wt%, 0.26 M) was purchased from Tokyo Ohka Kogyo. The molecular structures of these materials are presented in **Fig. 2-1**. The underlayer solutions were supplied by Nissan Chemical Corp. and were similar to those used in previous research, as shown in **Fig. 2-2**.[20]

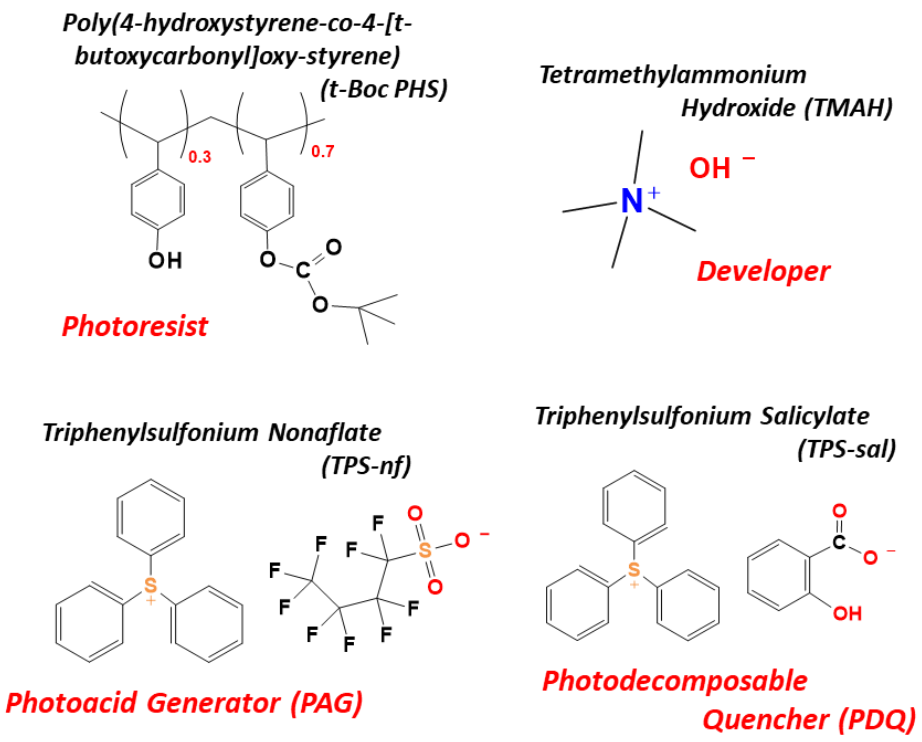

Fig. 2-1. Molecular structures of photoresist, developer, photoacid generator (PAG), and photodecomposable quencher (PDQ).

	None	NCX11085	NCX11086	NCX11087	NCX11088	NCX11089	NCX11090	NCX11286	NCX11287	NCX11288
	Au (Aurum)		F	CH_3	O CH_3	OH	O C_4H_9	I		F_3C CF_3
Polar	2.5	9.9	8.5	7.7	10.8	16.9	4.3	6.2	6.8	5.2
Dispersion	36.9	35.4	32.7	34.2	35.1	34.4	33.1	42.8	39.1	19.3
Ratio	0.067	0.280	0.260	0.389	0.308	0.491	0.130	0.145	0.174	0.269
Group	B	A	A	B	C	B	C	C	C	A

Fig. 2-2. Chemical structures of end groups and surface free energy (SFE) of underlayers in unit of mJ/m^2. "Ratio" represents the ratio of polar to dispersion component of SFE. The definition of "Group" has been described in the text.

Underlayers of approximately 40 nm thickness were spin-coated on QCM substrates and prebaked at 205 °C for 60 s. The as-prepared photoresist solution was spin-coated on the underlayers or directly on the QCM substrates to obtain photoresist films of approximately 200 nm thickness, which were then prebaked at 90 °C for 90 s. The as-prepared sample was irradiated using a UV lamp at a wavelength of 254 nm (SLUV-6, As One). The exposure doses were 20, 30,

40, 50, 55, 60, 65, 70, and 80 mJ/cm^2. PEB was performed at 60 °C. For exposure doses below 40 mJ/cm^2, the baking time was 90 s; the baking time was increased by 30 s for each dose increase of 10 mJ/cm^2, to obtain a linear dependence of the reaction extent on the exposure dose, as will be explained later along with experimental results. The reactions of *t*-Boc PHS, TPS-nf, and TPS-sal during UV exposure are presented in **Fig. 2-3**.[21-23] Protons were generated by the decomposition of PAG after UV exposure, which then activated the transformation of the polymer molecules. The existence of PDQ within the polymer films restricted the propagation of the as-formed protons among the *t*-Boc PHS. The QCM substrates were immersed in the TMAH aqueous developers, and the dissolution behaviors were detected using a QCM-based development analyzer (Litho Tech Japan, RDA-Qz3).[24] The film thicknesses before and after UV exposure and after development were measured using an ellipsometer (Meiwafosis FS-1).

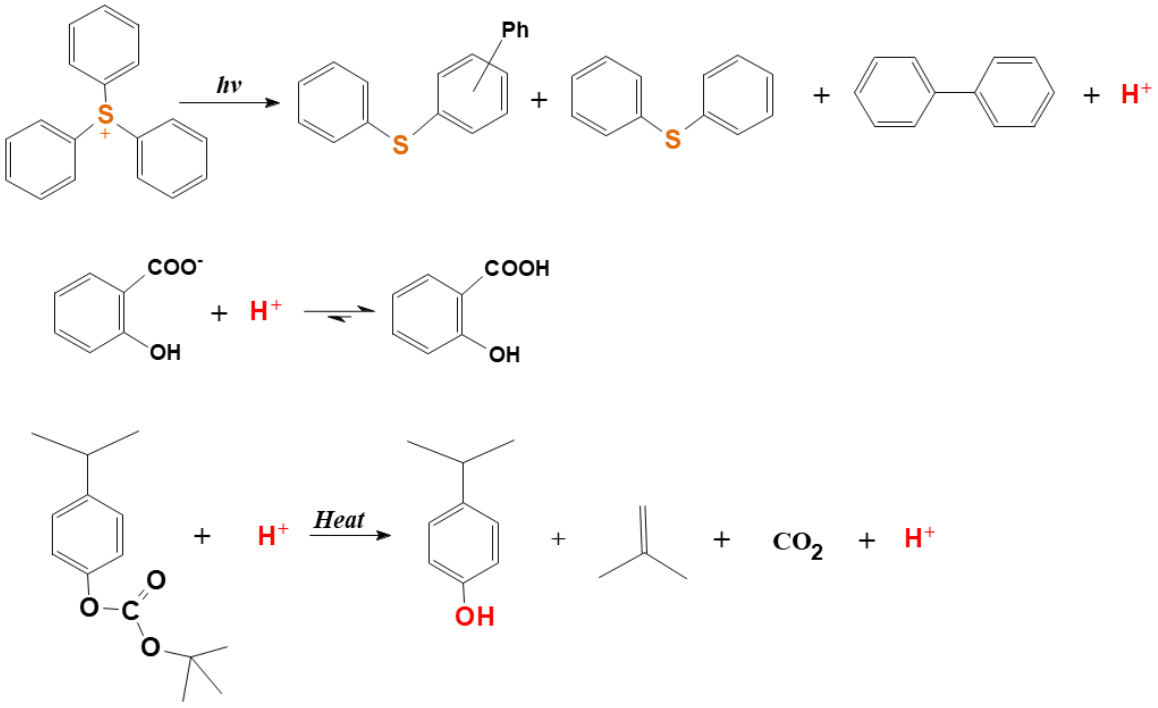

Fig. 2-3. Reactions of photoresist (*t*-BOC PHS, PAG, and PDQ) under exposure to UV light at a wavelength of 254 nm.

The QCM method can detect the dissolution details of solid on the substrate during the dissolution process. Because of the piezoelectric nature of the quartz crystal, the weight change and viscoelasticity of the films could be determined from the frequency (Δf) and impedance (Z).[25,26] The variation in the frequency corresponded to the swelling and dissolution of polymer films, while the impedance change was related to the viscoelasticity of the film and viscosity of

the contacting liquid on the QCM substrate, which was attributed to the power dissipation due to the propagation of the damped shear wave into the liquid around the oscillating QCM substrate surface.[27] In previous researches, the QCM method was applied to detect the dissolution behavior of photoresists in different developers.[28-31]

The SFE is obtained by the contact angles through the Owens, Wendt, Rabel, and Kaelble method.[32,33] In this study, two reference liquid—water and diiodomethane—were used to measure the dispersion component (γ^d) and polar component (γ^p). γ^d and γ^p of water were 51.0 and 21.8 mJ/m^2, respectively, and of diiodomethane were 2.3 and 48.5 mJ/m^2, respectively.

2-3. Results and Discussion

With an increase in the dose, the *t*-Boc PHS within the polymer films was continuously transferred to the PHS, accompanied by the release of CO_2, which decreased the film thickness. Such a decrease in thickness could demonstrate the degree of reaction of *t*-Boc PHS. Meanwhile, the SFE components of surface free energy in *t*-Boc PHS, the polar and dispersion component, varied with reaction progress. The decreased thickness and variation of the surface free energy with the dose are shown in **Fig. 2-4**.

As shown in **Fig. 2-4(a)**, at a dose smaller than 65 mJ/cm^2, the decrease in film thickness showed a linear tendency when adjusting the PEB time, as indicated in the experimental section. The decrease rate of film slowed down and reached the maximum descend as approximately 26% even after a long PEB time, indicating that the reaction of *t*-Boc PHS was complete and that it was completely transferred to the PHS. In the high-dose area of 60–80 mJ/cm^2, the difference in decrease was similar, while in the low-dose area of 20–40 mJ/cm^2, the decrease in film thickness (in other words, the degree of reaction) showed a great difference. This dispersion (stochasticity) was probably due to the low degree of reaction. The standard deviation of the decrease in film thickness is presented in **Fig. 2-4(b)**. The dose-dependence of SFE differed from that of the film thickness. As shown in **Fig. 2-4(c)**, at the dose smaller than 30 mJ/cm^2, the polar component increased rapidly, whereas it slowed and reached approximately 28 mJ/m^2 at doses larger than 30 mJ/cm^2. The dispersion component gradually decreased from approximately 35 mJ/m^2 to approximately 31 mJ/m^2 without a significant rate change when the exposure dose was increased.

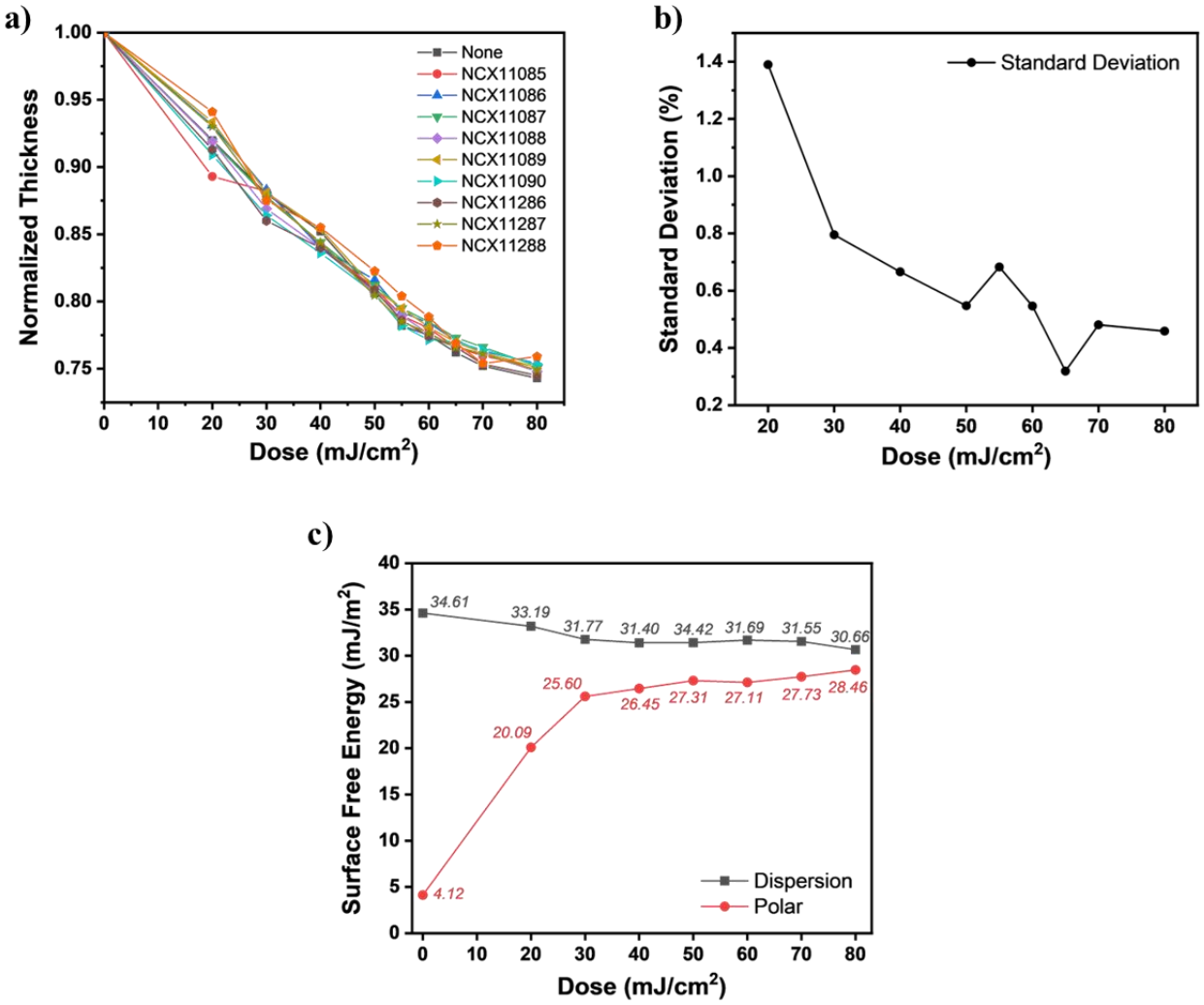

Fig. 2-4. (a) Dependence of film thickness on exposure dose for the samples with different underlayers. (b) Dependence of standard deviation of decreased film thickness on exposure dose. (c) Dependence of surface free energy of polymer film without the underlayer on exposure dose. The black and red dots are the dispersion (γ^d) and polar (γ^p) components, respectively.

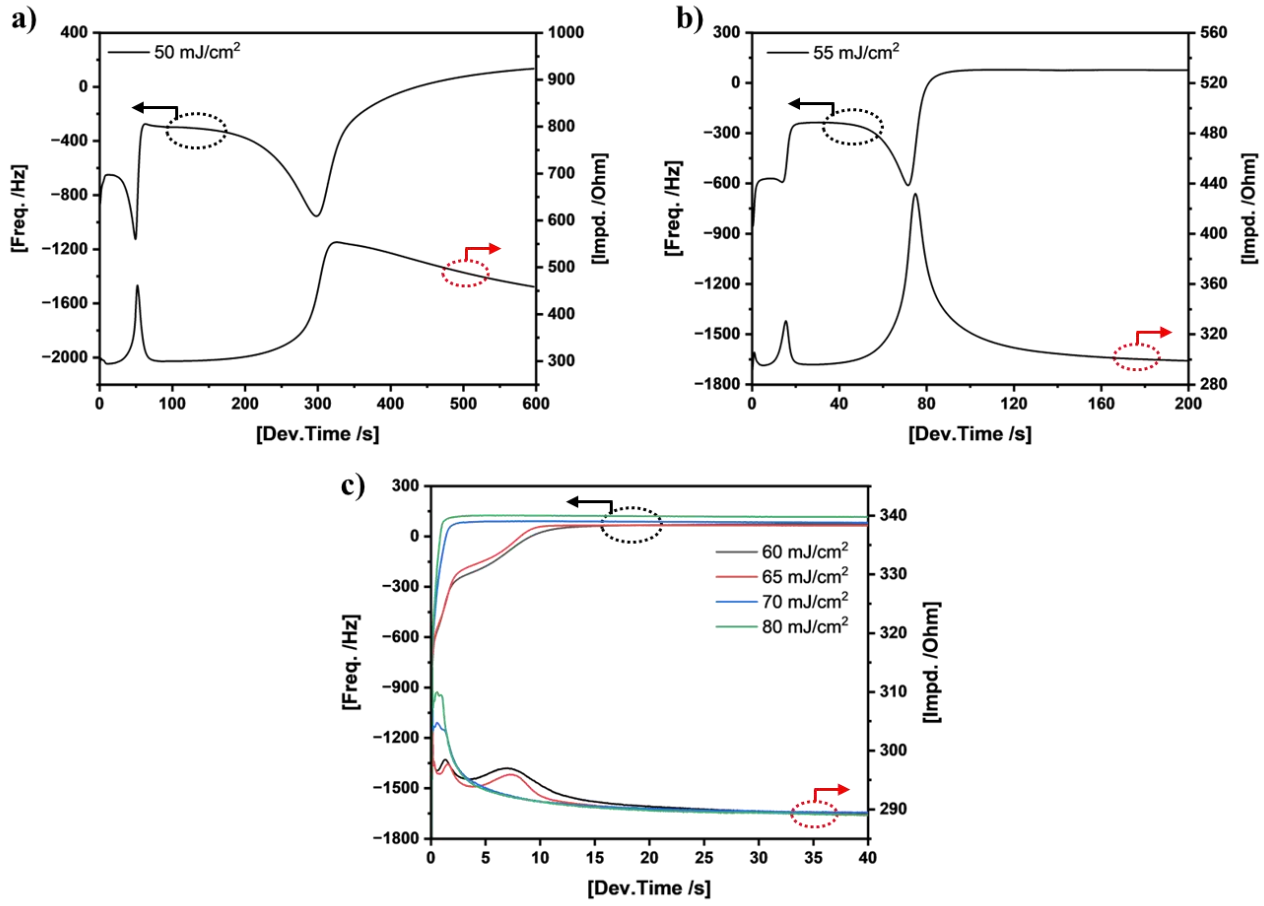

Fig. 2-5. Dissolution behaviors of photoresist films without the underlayer in the TMAH aqueous solution. The exposure doses were a) 50, b) 55, and c) 60–80 mJ/cm^2.

The dissolution behavior of the polymer film without an underlayer is presented in **Fig. 2-5**. The behavior varied with the exposure dose and could be classified into three types: I) for the dose from 20 to 40 mJ/cm^2, at which the sample was almost insoluble; II) for the dose from 50 to 55 mJ/cm^2, at which the sample started to dissolve but at a low speed, as shown in **Figs. 2-5(a)** and **2-5(b)**; III) for the dose from 60 to 80 mJ/cm^2, at which the sample rapidly dissolved, as shown in **Fig. 2-5(c)**. For Type II, a rapid drop in the frequency was observed owing to the formation of a transient gel layer, indicating severe swelling of the film. In addition, the surface and bulk layers differently dissolved at low speeds, as shown in **Figs. 2-5(a)** and **2-5(b)**. The first peak at approximately 50 s corresponded to the dissolution of the film near the surface, and the second peak corresponded to the dissolution of the bulk layer. The existence of a transient gel layer could be observed by the variation of impedance of over approximately 100 Ω. A transient gel layer with a large thickness was produced owing to the low dissolution ability and great

penetration of the developer. For Type III, no obvious swelling occurred in the polymer films. However, the dissolution behavior differed according to the exposure dose, as shown in **Fig. 2-5(c)**. In the case of samples with exposure doses of 60 and 65 mJ/cm^2, owing to the penetration limitation of the developer, the separation between two layers still existed, similar to the case in Type II. The dissolution of samples with exposure doses of 70 and 80 mJ/cm^2 were monotonic without separated peaks. A similar trend in the dose dependence was observed in the impedance change. Upon exposure to 70 and 80 mJ/cm^2 deep UV (DUV) light, the maximum impedance change (approximately 20 Ω) was greater than that upon the exposure to 60 and 65 mJ/cm^2 DUV light (approximately 5 Ω). This greater change in the case of samples exposed to 70 and 80 mJ/cm^2 indicated that the film dissolved rapidly and that the polymer concentration around the interface between the liquid and film became high because of the diffusion limitation of the developer. Hereafter, the dissolution behavior observed for the samples irradiated with 60 and 65 mJ/cm^2 is referred to as Type III(a), whereas that observed for the samples irradiated with 70 and 80 mJ/cm^2 is referred to as Type III(b). Type I samples are insoluble. Type II samples exhibit two negative peaks in the frequency chart and two positive peaks in the impedance chart. Type III(a) samples exhibit a shoulder in the frequency chart and two positive peaks in the impedance chart. Type III(b) samples show a monotonic increase in frequency. It should be noted that an interface layer exists between the polymer bulk layer and QCM substrate. This has a significant influence on the frequency variation, corresponding to the curved part after the straight line of bulk-layer dissolution and before the plain line of completed dissolution.

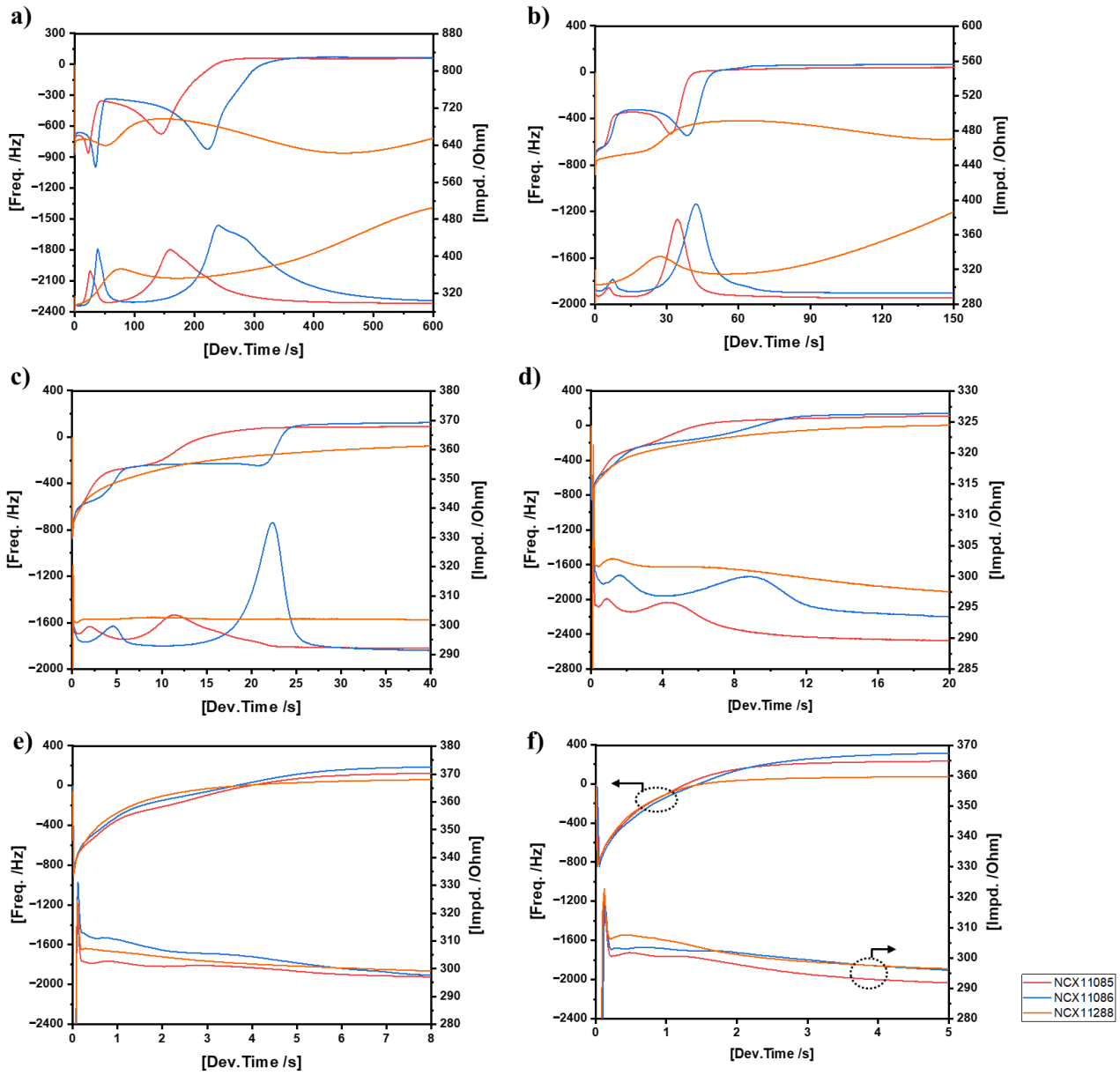

Fig. 2-6. Dissolution behaviors of photoresist films with the underlayer (Group A) in TMAH aqueous solution. The exposure doses were a) 50, b) 55, c) 60, d) 65, e) 70**,** and f) 80 mJ/cm^2.

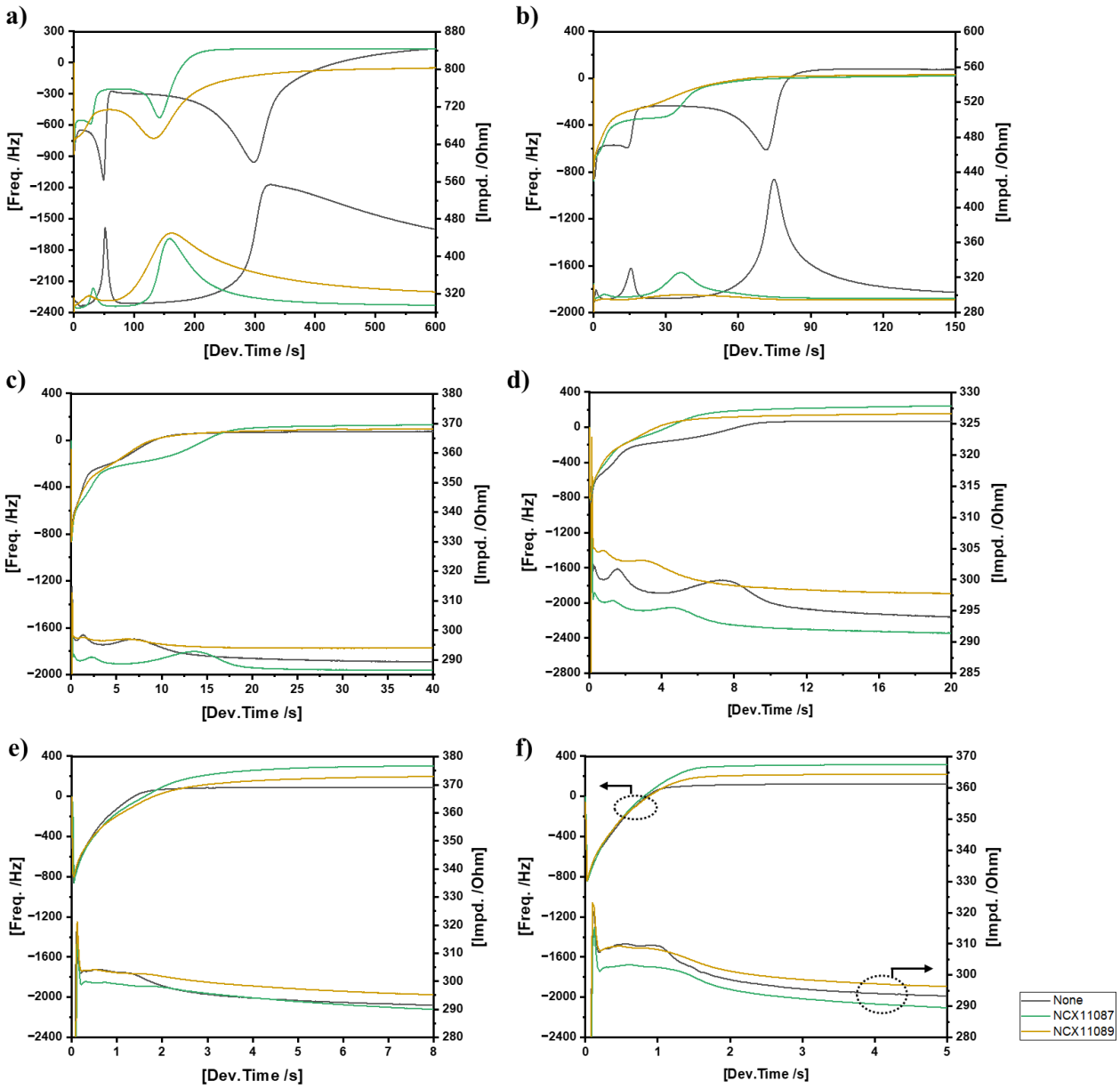

Fig. 2-7. Dissolution behaviors of photoresist films with underlayer (Group B) in TMAH aqueous solution. The exposure doses were a) 50, b) 55, c) 60, d) 65, e) 70, and f) 80 mJ/cm^2.

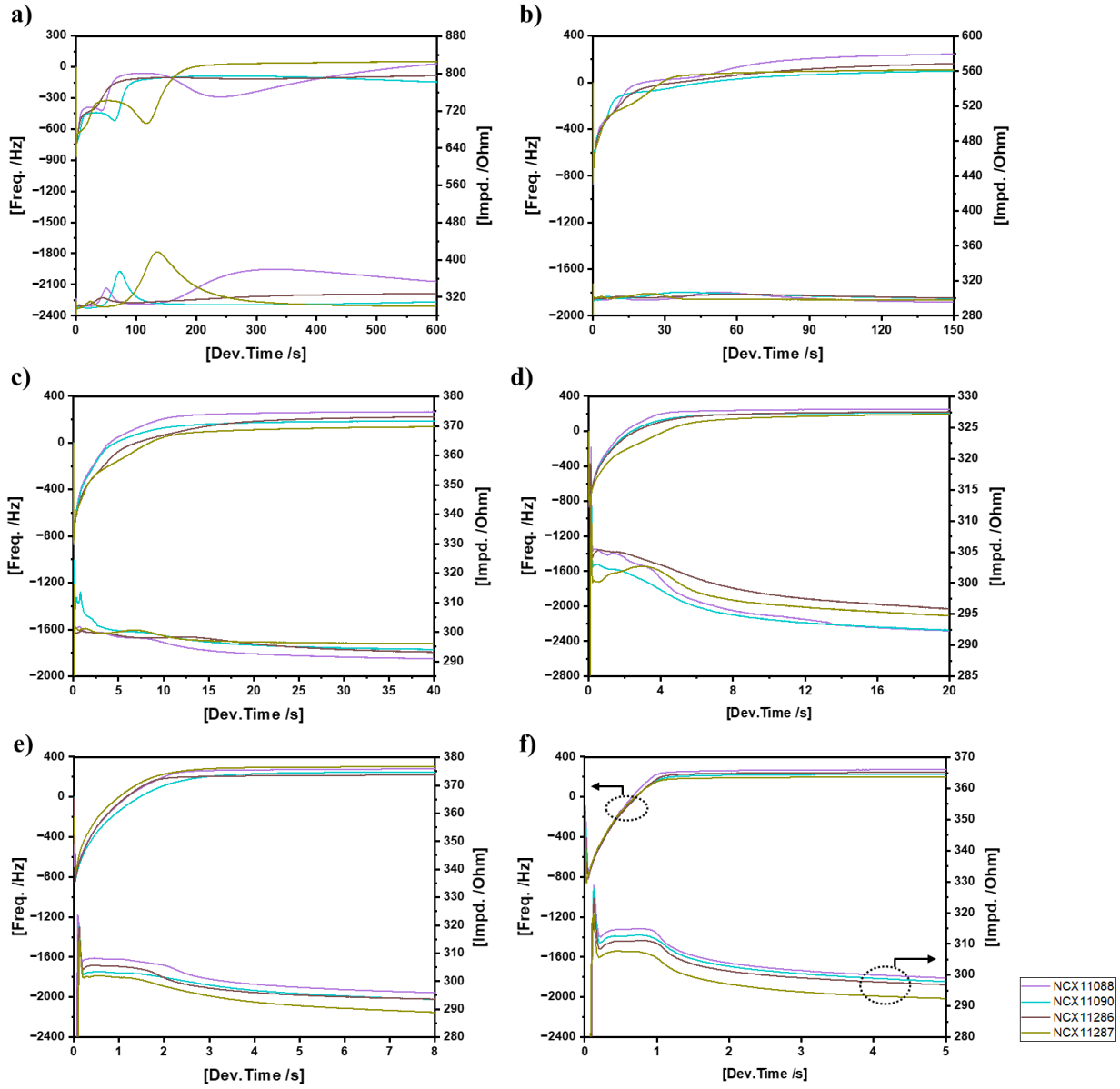

Fig. 2-8. Dissolution behaviors of photoresist films with underlayer (Group C) in TMAH aqueous solution. The exposure doses were a) 50, b) 55, c) 60, d) 65, e) 70, and f) 80 mJ/cm^2.

The dissolution behavior of a polymer film with an underlayer is more complicated than that without an underlayer. The underlayers are divided into three groups, as shown in **Figs. 2-6** to **2-8**, The groups are classified by the dissolution rate at an exposure dose of 80 mJ/cm^2 into A) ones with a rate lower than None (the samples without an underlayer), which are NCX11085, NCX11086, and NCX11288; B) ones with a rate similar to None, which are NCX11087 and NCX11089; and C) ones with a rate greater than None, which are NCX11088, NCX11090, NCX11286, and NCX11287. These classified groups are called Groups A, B, and C, respectively,

for convenience, and are summarized in **Fig. 2-2**.

First, we discuss the overall dissolution kinetics presented in **Figs. 2-6** to **2-8**. Several points should be noticed after the attachment of the underlayer to the QCM substrates. For Type II (typically observed in samples with 50 and 55 mJ/cm^2 exposure doses), because of the underlayer, the film swelling improved according to the variations in the frequency and impedance in **Figs. 2-6(a)**, **2-6(b)**, **2-7(a)**, **2-7(b)**, **2-8(a)**, and **2-8(b)**; however, NCX11288 showed a slower dissolution process than the others. This suggested a strong interaction between NCX11288 and the resist film. Similarly, NCX11288 exhibited the slowest speed during the dissolution process for samples with 60 and 65 mJ/cm^2 exposure doses, as shown in **Figs. 2-6(c)** and **2-6(d)**. The dissolution behaviors of the other types of underlayers were different. In the case of samples with an exposure dose of 60 mJ/cm^2, the dissolution behavior corresponded to Type III(a) for the underlayers NCX11085, NCX11086, NCX11087, and NCX11287, whereas those of the other underlayers belonged to Type III(b). Among the samples exposed to 65 mJ/cm^2, NCX11085 and NCX11086 still exhibited Type III(a) dissolution behavior. At high doses (70 and 80 mJ/cm^2), no significant differences were observed in dissolution behavior. All samples exhibited Type III(b) behavior, as presented in **Figs. 2-6(e)**, **2-6(f)**, **2-7(e)**, **2-7(f)**, **2-8(e)**, and **2-8(f)**. Although the data were scattered, the dissolution mode tended to change from Type II to Type III(a) and Type III(b) when the underlayer changed from one in Group A to one in Groups B or C. Such data scattering was consistent with the variation in the reaction degree, as shown in **Fig. 2-4(b)**. The first peaks in Types II and III(a) were affected by the basic compounds in the atmosphere. This effect was probably the main cause of the considerable data variation (scattering) because we could not control the concentration of ambient basic compounds in our laboratory. However, a weak dependence of the first peak on the underlayer group was observed when the underlayer changed from Group A to C.

In practice, the categories of groups are highly related to the SFE. It has been reported that the dissolution kinetics of polymer films are affected by the SFE of the underlayer.[18,20] However, it is difficult to find a clear correlation between them because the polar and nonpolar components of the SFE affect the dissolution kinetics of the photoresist film differently. The ratio of polar to dispersion components has been reported to be a good indicator, if not an ideal indicator, for describing the relationship between the dissolution kinetics of the photoresist and underlayer.[20] For convenience, the ratio of polar to dispersion components is hereafter referred to as the SFE ratio. The SFE ratio in Group A was 0.26–0.28; for Group B, it was 0.39 – 0.49; and for the last group, Group C, it was lower than 0.18 except for NCX11088 (the SFE ratio of 0.31).

Considering that the SFE ratio of the polymer film changed from 0.79 to 0.93 upon increasing the exposure dose from 50 to 80 mJ/cm^2 and the ratio of the underlayer in group C was below 0.18, the interaction between the underlayer and polymer film was weak, which was beneficial to the dissolution process. On the contrary, the strong interaction between the photoresist film and underlayer increased the glass transition temperature T_g of the photoresist film and suppressed acid diffusion.[34-37] The SFE ratio of the photoresist film before exposure to UV light was 0.12. Therefore, the degree of progress of the chemical reaction near the underlayer was considered to have increased with the SFE ratio. Owing to these two different effects of the underlayer, the change in the dissolution mode from Type II to Type III(b) for Group A was considered to be the least sensitive to the exposure dose, among the underlayer groups. This hypothesis may also explain the effects of NCX11088. In the case of the specific performance of NCX11088, owing to the similarity of the chemical structure to the other underlayers, the methoxy group in the underlayer copolymer was speculated to be the main reason why NCX11088 (SFE ratio of 0.31) was categorized as Group C. **Figure 2-9** shows the proton affinities of the end groups of the underlayers.[38] It was reported that the proton generated upon exposure to radiation migrated via proton acceptors, typically, the hydroxyl group of the phenol unit of the photoresist polymer.[39-41] If the proton affinity of the proton acceptor was sufficiently high, proton migration was terminated. This was the role of a quencher, whose proton affinity is typically greater than 900 kJ/mol. NCX11088, which has a proton affinity similar to that of phenol, likely functioned as a proton acceptor for proton migration and promoted chemical reactions near the underlayer. For the other underlayers, the proton affinity was too low to function as a proton acceptor in the presence of phenol units.

	Benzene	Fluoro-Benzene	Toluene	Anisole	Benzyl Alcohol	Butyl Phenyl Ether	1-Iodo-2-Metylbenzen	Naphthalene	1,3-Bis(trifluoromethyl) Benzene	Phenol
									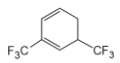	
Proton Affinity	750.4	755.9	784.0	839.6	778.3	-	780.3	802.9	-	817.3

Fig. 2-9. Proton affinity of model compounds in kJ/mol.[38] Phenol is a model compound of PHS.

In the photoresist process, the dissolution kinetics at the boundary between the resist patterns and spaces, namely, the boundary between the soluble and insoluble regions, are critical to the pattern quality. The dissolution kinetics of such a boundary (50–60 mJ/cm^2 for the photoresist

used in this study) are significantly affected by the underlayer. However, the effect of the underlayers was complex, although the SFE ratio explained their effects to some extent. The reason for this complicated effect was speculated as follows. The polar and nonpolar components of the underlayer SFE affected the adhesion of the photoresist films differently. Although the strength of adhesion directly affected the dissolution behavior of the resist films, it also indirectly affected the dissolution behavior by affecting the acid diffusion in the photoresist films. The proton affinity of the underlayer affected the proton migration during PEB. Furthermore, the effect of stochasticity on the dissolution kinetics increased with decreasing exposure doses, as discussed previously. In electron-beam and EUV lithography processes, low-energy secondary electrons generated in the underlayers were reported to affect the photoresist performance in addition to the factors discussed here.[42-44)]

2-4. Conclusion

The dissolution behavior of the three-component photoresist *t*-Boc PHS/TPS-nf/TPS-sal with an underlayer in the TMAH aqueous solution was analyzed in this study. The underlayer had a complex effect on the photoresist during dissolution. In particular, the underlayer significantly affected the formation of the transient swelling layer and dissolution kinetics at an exposure dose close to the photoresist sensitivity, namely, at the critical exposure dose for solubilizing the photoresist films. For the photoresist used in this study, the dissolution kinetics was strongly (negatively from the viewpoint of photoresist performance) affected by the underlayers at an SFE ratio of 0.26–0.28. The results obtained in this study suggested that the adjustment of the polar and nonpolar components of the SFE of the underlayers was required in accordance with the chemical conditions of photoresist films at an exposure dose close to the photoresist sensitivity for the precise control of dissolution kinetics, namely, the pattern shape. Furthermore, the proton affinity of the end groups of the underlayers probably affected the progress of the acid-catalytic reaction, and thereby, the dissolution kinetics.

References

1) T. Itani, P. A. Gargini, P. P. Naulleau, and K. G. Ronse, Proc. SPIE **11147**, 1114701 (2019).
2) A. C. Gysen, C. W. Man, B. V. Meerten, H. V. Loo, E. V. Setten, S. Smith-Meerman, G. Yegen, D. D. Bruin, J. V. Schoot, R. Peeters, K. Bhattacharyya, G. Storms, and P Vanoppen, Proc. SPIE **PC13215**, PC132150 (2024).

3) V. Philipsen, A. Frommhold, D. Thakare, G. Libeert, I. Lee, J. H. Franke, J. Bekaert, L. V. Look, N. Pellens, P. D. Bisschop, R. Jonckheere, T. Kovalevich, V. Wiaux, and E. Hendrickx, Jpn. J. Appl. Phys. **63**, 040804 (2024).
4) N. Pellens, V. Philipsen, J. -H. Franke, K. Ronse, and E. Hendrickx, Proc. SPIE **13215**, 1321505 (2024).
5) R. Gronheid, A. V. Pret, and A. Burov, Proc. SPIE **12494**, 124940O (2023).
6) I. Lee, J. H. Franke, V. Philipsen, K. Ronse, S. D. Gendt, and E. Hendrickx, J. Micro/Nanopatterning, Mater. and Metrol. **22**, 043202 (2023).
7) H. J. Levinson, Jpn. J. Appl. Phys. **61**, SD0803 (2022).
8) T. Kozawa and S. Tagawa, Jpn. J. Appl. Phys. **49**, 030001 (2010).
9) T. Kozawa, J. J. Santillan, and T. Itani, Jpn. J. Appl. Phys. **52**, 076502 (2013).
10) P. D. Bisschop, J. Micro/Nanolithography, MEMS, and MOEMS **17**, 1 (2018).
11) L. S. Melvin, U. Welling, Y. Kandel, Z. A. Levinson, H. Taoka, H. J. Stock, and W. Demmerle, Jpn. J. Appl. Phys. **61**, SD1030 (2022).
12) J. J. S. Santillan, M. Harumoto, H. W. Stokes, C. Mori, Y. Tanaka, Y. Arisawa, T. Motono, M. Asai, and T. Itani, Proc. SPIE **11323**, 113231W (2020).
13) T. Kozawa, Jpn. J. Appl. Phys. **63**, 050101 (2024).
14) R. Sakamoto, B.-C. Ho, N. Fujitani, T. Endo, and R. Ohnishi, Proc. SPIE **7969**, 79692F (2011).
15) P. Vanelderen, N. Vandenbroeck, Y. Liang, V. V. Driessche, D. Guerrero, A. Chacko, D. D. Simone, and G. Vandenberghe, Proc. SPIE **11326**, 1132615 (2020).
16) R. Fallica, S. Chen, D. D. Simone, and H. S. Suh, J. Micro/Nanopatterning, Mater. Metrol. **21**, 34601 (2022).
17) M. Padmanaban, J. Cho, T. Kudo, S. Mullen, H. Yao, G. Noya, Y. Matsuura, Y. Ide, J. Li, and G. Pawlowski, Proc. SPIE **8682**, 868215 (2013).
18) T. Otsuka, Y. Jin, N. Tanaka, and T. Kozawa, Jpn. J. Appl. Phys. **61**, 056503 (2022).
19) Y. T. Ito and T. Kozawa, Jpn. J. Appl. Phys. **61**, 016502 (2022).
20) J. Wang and T. Kozawa, Jpn. J. Appl. Phys. **63**, 096502 (2024).
21) S. Kobayashi, J. J. Santillan, H. Oizumi, and T. Itani, Microelectron. Eng. **86**, 479 (2009).
22) E. Despagnet-Ayoub, W. W. Kramer, W. Sattler, A. Sattler, P. J. Labeaume, J. W. Thackeray, J. F. Cameron, T. Cardolaccia, A. A. Rachford, J. R. Winkler, and H. B. Gray, Photochem. Photobiological Sci. **17**, 27 (2018).
23) Y. Miyake, M. Isono, and A. Sekiguchi, J. Photopolym. Sci. Technol. **14**, 463 (2001).

24) A. Sekiguchi, J. Photopolym. Sci. Technol. **26**, 479 (2013).
25) S. W. Lee, W. D. Hinsberg, and K. K. Kanazawa, Anal. Chem. **74**, 125 (2002).
26) K. K. Kanazawa, Faraday Discuss. **107**, 77 (1997).
27) M. V. Voinova, M. Rodahl, M. Jonson, and B. Kasemo, Physica Scripta **59**, 391 (1999).
28) Y. T. Ito, H. Betsumiya, T. Kozawa, K. Sakamoto, and M. Muramatsu, Jpn. J. Appl. Phys. **61**, 066506 (2022).
29) H. Betsumiya, Y. T. Ito, T. Kozawa, K. Sakamoto, and M. Muramatsu, Jpn. J. Appl. Phys. **62**, 036503 (2023).
30) M. Harumoto, J. J. Santillan, T. Itani, and T. Kozawa, Jpn. J. Appl. Phys. **61**, 056506 (2022).
31) J. Wang and T. Kozawa, Jpn. J. Appl. Phys. **63**, 076503 (2024).
32) D. K. Owens and R. C. Wendt, J. Appl. Polym. Sci. **13**, 1741 (1969).
33) D. H. Kaelble, J. Adhesion **2**, 66 (1970).
34) K. C. Tseng, N. J. Turro, and C. J. Durning, Phys. Rev. E **61**, 1800 (2000).
35) D. S. Fryer, P. F. Nealey, and J. J. Pablo, J. Vac. Sci. Technol. B **18**, 3376 (2000).
36) D. R. Medeiros, W. M. Moreau, K. Petrillo, M. Chauhan, W. S. Huang, C. Magg, D. Goldfarb, M. Angelopoulos, and P. Nealey, Proc. SPIE **4345**, 241 (2001).
37) L. Singh, P. J. Ludovice, and C. L. Henderson, Proc. SPIE **5039**, 1008 (2003).
38) CRC Handbook of Chemistry and Physics 97th, W. M. Haynes (ed.) (CRC Press Inc, Boca Raton, FL, 2016-2017) p. 10–170.
39) K. Natsuda, T. Kozawa, K. Okamoto, and S. Tagawa, Jpn. J. Appl. Phys. **45**, L1256 (2006).
40) K. Natsuda, T. Kozawa, K. Okamoto, and S. Tagawa, Jpn. J. Appl. Phys. **46**, 7285 (2007).
41) H. Yamamoto, T. Kozawa, A. Nakano, K. Okamoto, Y. Yamamoto, T. Ando, M. Sato, H. Komano, and S. Tagawa, Jpn. J. Appl. Phys. **43**, L848 (2004).
42) T. Kozawa, S. Tagawa, R. Ohnishi, T. Endo, and R. Sakamoto, Jpn. J. Appl. Phys. **50**, 016504 (2011).
43) T. Kozawa and T. Tamura, Jpn. J. Appl. Phys. **60**, 086503 (2021).
44) T. Kozawa and T. Tamura, Jpn. J. Appl. Phys. **60**, 126504 (2021).

Chapter 3 Dissolution kinetics of poly(4-hydroxystyrene) partially protected by tert-butoxycarbonyl (t-Boc) group in alkyl-trimethyl-ammonium hydroxide (A-TMAH) aqueous developers

3-1. Introduction

The extremely large integration and mass production of semiconductor devices with low manufacturing costs are in demand for the advancement of information technology. The advanced extreme ultraviolet (EUV) irradiation with the wavelength of 13.5 nm has been applied in the industry since 2019.[1)] To realize the further miniaturization, a high-performance optical tool with numerical aperture (NA) of 0.55 has been available recently. The goal of this high NA tool is to obtain optical images with a pitch of 16 nm by 2031.[3)] However, many problems remain to be solved before the full potential of such a high NA tool could be realized. Stochastic defects generated owing to the swelling and non-uniform dissolution of the photoresist polymer film during the development are still an intractable issue.[2-5)] The development processes for photoresist films, including the swelling process, play an important role in the production of semiconductor devices.

The chemically amplified resists (CARs) (polymer-type photoresists) have been widely used in industry and have a high potential owing to their highly sensitive reaction mechanism.[6,7)]. The PHS is a typical base polymer of CARs. In typical CARs, some hydroxyl groups are substituted by *t*-butoxycarbonyl groups to generate the difference of solubility before and after exposure to the light source. To dissolve the soluble part of the photoresist film and form a certain pattern, the prepared photoresist film is immersed in the developer. Currently, 2.38 wt% (0.26 N) tetramethyl-ammonium hydroxide (TMAH) aqueous solution is utilized as the standard developer in industrial manufacture.

Even though the TMAH aqueous solution has long been used as the developer for polymer photoresists, many problems remain to be overcome. Metal oxide photoresists are potential candidates for the next generation; however, the conventional developer is not applicable to the development process for metal oxide photoresists.[8,9)] On the other hand, TMAH is highly toxic to organisms. In the previous studies, aqueous solutions of other tetraalkylammonium hydroxide (TAAH) such as tetraethylammonium hydroxide (TEAH), tetrapropylammonium hydroxide (TProAH), and tetrabutylammonium hydroxide (TBAH) were applied to the development of CARs to study the dissolution dynamics.[9-16)] Although the toxicity decreases with the elongation of side chains, the elongation will likely induce the swelling of films owing to the sluggish

penetration of developers, resulting in the generation of pattern defects of photoresist films after the development.[15,16] It remains a challenge to find a new developer with low toxicity and similar performance to the TMAH aqueous solution.

Recently, the ethyl-trimethyl-amonium hydroxide (E-TMAH) aqueous developer was reported to be compatible with the standard TMAH developer and to mitigate resist-based stochastic defects while maintaining lithographic performance.[17,18] In this chapter, the dissolution kinetics of alkyl-trimethyl-ammonium hydroxide (A-TMAH) aqueous solution, where one of the methyl chains in TMAH was substituted by a long alkyl chain to decrease its biotoxicity, was investigated. The t-Boc PHS was used as the photoresist, and the quartz crystal microbalance (QCM) method was applied to the observation of the dissolution process to determine the dissolution kinetics during the development. The QCM method is widely used to study the dissolution dynamics of photoresist during the development.[19,20] In the QCM method, the properties of film can be analyzed on the basis of utilizing the vibration of a quartz crystal. The stages of film dissolution are generally divided into three: film swelling due to the solvent permeation, the solvation, and the diffusion of the dissolved film into the solution. A-TMAH in addition to E-TMAH was first utilized as a novel organic alkali for developers. One of the alkyl chains in TMAH was substituted by propyl and butyl groups, and the resulting organic alkalis were named P- and B-TMAH, respectively. The conventional TMAH and TEAH aqueous solutions were also used to compare their dissolution processes with those of the above developers. TMAH and E-, P-, and B-TMAH developers are hereafter collectively called A-TMAH developers.

3-2. Experiments

PHS (weight-average molecular weight, M_w = 11000) and propylene glycol monomethyl ether acetate (PGMEA) were purchased from Sigma-Aldrich. The hydroxyl group of PHS was partially protected by *t*-Boc groups. The protection ratios of PHSs were 30, 50, and 70 mol%. The PHSs with 0, 30, 50, 70 mol% protection ratios were named 0%, 30%, 50% and 70% *t*-Boc PHS, respectively, for simplicity. Five types of 0.26 N tetraalkyl ammonium hydroxide aqueous developer with different alkyl chains were supplied by Tokuyama Corporation. The molecular structures of *t*-Boc PHS and developers are shown in **Fig. 3-1**.

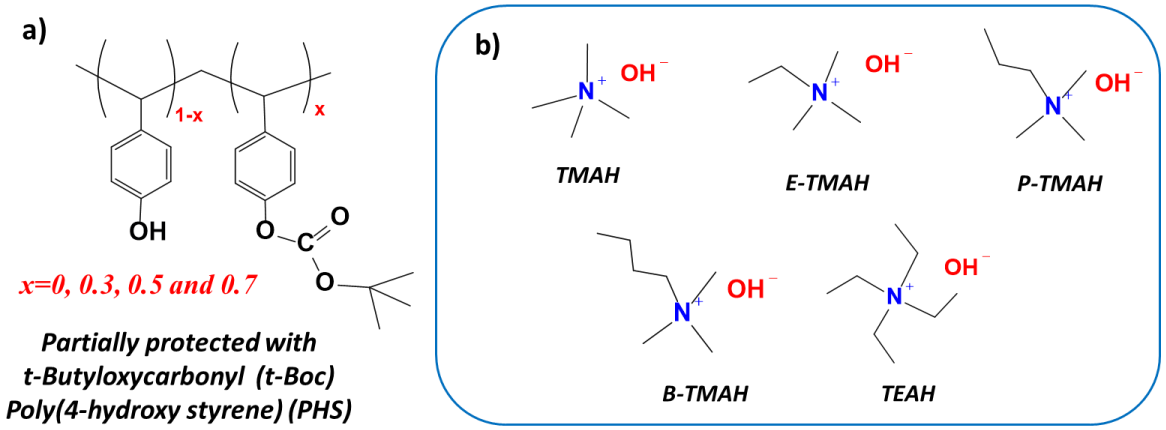

Fig. 3-1. The molecular structures of (a) *t*-Boc PHS and (b) A-TMAH and TEAH.

The *t*-Boc PHS powders were dissolved in the PGMEA, and concentrations of solutions were adjusted to obtain the films with thicknesses of 50 and 200 nm. The solutions were spin-coated on QCM substrates and then prebaked at 90 °C for 90 s. The obtained films were developed in the developers at 23 °C and then rinsed in water. The dissolution kinetics of films in different developers were observed using a QCM-based development analyzer (Litho Tech Japan, RDA-Qz3). Both resonance frequency change (Δf) and electrical impedance (Z) were measured. The thicknesses before and after the development were measured using an ellipsometer (Meiwafosis FS-1).

The 0 and 30% *t*-Boc PHS powders were dissolved in five aqueous developers to prepare 1, 2, and 3 wt% solutions, as well as the 5 wt% saturated solution. The electrical impedance (Z) of as-prepared solutions and pristine developers was also measured using the QCM-based development analyzer.

The QCM method is a rapid, real-time, and effective method of detecting the dissolution kinetics of films during their development. The QCM substrate is composed of a crystal quartz sandwiched between Au electrodes. Due to the piezoelectric properties of the quartz crystal, the weight change and viscoelastic property of films could be observed from the measured Δf and Z.[21,22)]

The Δf during the development is corresponded to the weight loss of the film. The relationship between the mass change and frequency changes of an oscillating crystal was introduced by Sauerbrey as:[23)]

$$\Delta f = -\frac{2{f_0}^2}{A\sqrt{\rho_q \mu_q}}\Delta m, \quad (1)$$

where the Δf, f_0, Δm, A, ρ_q, and μ_q are the frequency change, the resonant frequency of the

unloaded QCM substrate, the mass change of the material on the substrate, the piezoelectrically active crystal area, the density of quartz, and the shear modulus of the quartz used as the AT-cut crystal, respectively. However, Eq. (1) is only restricted to a uniform, rigid, and thin film. Further investigation was applied in the condition of a Newtonian liquid.[24] The relationship between the Δf of a crystal resonator and Newtonian liquid could be determined by calculating the equation:

$$\Delta f = f_0^{\frac{3}{2}}(\eta\rho/\pi\rho_q\mu_q)^{\frac{1}{2}}, \quad (2)$$

where ρ and η are the density and shear viscosity of the liquid, respectively. Even though the above equation describes the relationship between the resonance frequency of viscoelastic films and Newtonian liquid, another approach is required for the explanation of impedance change.

In general, the impedance changes during the development are attributed to the power dissipation due to the propagation of damped shear waves into the liquid around the oscillating QCM substrate surface.[25] Martin et al. introduced the Butterworth-Van Dyke (BVD) equivalent circuit to describe the relationship between the viscoelastic properties of films and the loaded Newtonian liquid as:[26]

$$R_{load} = \frac{\omega_s L}{\pi}\sqrt{\frac{2\omega_s\rho\eta}{\bar{c}_{66}\rho_q}}, \quad (3)$$

where ω_s is the series resonant angular frequency of the quartz plate, L is the motional inductance of the unperturbed quartz resonator, and $\bar{c}_{66}$ is the elastic constant of piezoelectrically stiff quartz. In short, the impedance (Z) during the development in Eq. (3) is proportional to the square root of the density-viscosity product of the contacting liquid, $Z \sim (\rho\eta)^{0.5}$.

To obtain the diffusion constant of polymer in the developer, the dynamic light scattering (DLS) was introduced. Through the scattering pattern fluctuating over time, the size of dissolved polymer and their distribution could be measured. The size mentioned above was called the hydrodynamic radius (R_h). Based on the Stokes–Einstein–Sutherland equation, the diffusion constant (D) could be calculated from the R_h of the polymers and the viscosity of solvent (η_s) as follows:

$$D = \frac{k_B T}{6\pi\eta_s R_h}, \quad (4)$$

Where k_B, T, η_s and R_h are the Boltzmann constant, the absolute temperature, the viscosity of solvent and the hydrodynamic radius of dissolved polymer, respectively.

3-3. Results and Discussion

The *t*-Boc PHS films of 50 and 200 nm thicknesses were dissolved in different developers. The dissolution kinetics were recorded, as shown in **Figs. 3-2** and **Figs. 3-3**. The frequency changes correspond to the dissolution of films during their development, whereas the impedances change are related to the viscosity of the solution surrounding the films. According to previous reports, the dissolution kinetics varied with the film thickness and protection ratio of PHS,[16,27] consistent with the results of our study. The 50 and 70% *t*-Boc PHS films did not dissolve during the development regardless of thickness, whereas the swelling behaviors of the films caused by the developer permeation were observed [**Figs. 3-2(e)-(h)** and **3-3(e)-(h)]**. The dissolution kinetics of 0 and 30% *t*-Boc PHS films were complex.

In the cases of 0% *t*-Boc PHS films of 200 nm thickness and 30% *t*-Boc PHS films with 50 and 200 nm thicknesses, two peaks appeared during the impedance changes [**Figs. 3-2(d)**, **3-3(b)**, and **3-3(d)**], indicating at least two dissolution processes existed. The first peak reflects the dissolution kinetics at the initial surface of the resist film. The second peak reflects the dissolution kinetics near the substrate. Such phenomena were caused by differences in dissolution properties between the bulk and near-interface layers in the polymer film, derived from the interfacial effect at the resist surface and bottom.[28,29] However, owing to the limited time resolution of development analyzer and the over-rapid dissolution process, the effects at the two interfaces were not separately observed in the 0% *t*-Boc PHS films of 50 nm, as shown in Fig. 3-2(b).

On the other hand, a novel consequence was observed in the dissolution rate of *t*-Boc PHS films. For the 0 and 30% *t*-Boc PHS films, the dissolution rates were the lowest in TEAH solution among the developers used [**Figs. 3-2(a)-(d)** and **3-3(a)-(d)**]. For the 0% *t*-BOC PHS films of 50 nm, the order of dissolution rates among A-TMAH developers was unclear owing to the insufficient time resolution, as shown in **Figs. 3-2(a)** and **(b)**. At the film thickness of 200 nm, it was clearly observed that the dissolution rate gradually decreased with the elongation of one alkyl chain of tetramethyl ammonium cations, as shown in **Figs. 3-3(a)** and **(b)**. For the 30% *t*-Boc PHS films, the dissolution rate tended to increase with alkyl chain length, as shown in **Figs. 3-2(c)**, **3-2(d)**, **3-3(c)**, and **3-3(d)**, although the difference was insignificant.

Interestingly, the inflection points of peak impedance showed characteristic behavior, especially for the four types of ATMAH developers. The peak impedance in TEAH developer was lower than that in the TMAH developer, consistent with previous reports from our group.[16,30] The relative relationship among the peak impedances observed during the development of 0% *t*-

Boc PHS films of 50 nm in the A-TMAH developers was unclear owing to the insufficient time resolution, as shown in **Fig. 3-2(b)**. For the 0% *t*-Boc PHS films of 200 nm, the peak impedance in the E-, P-, and B-TMAH developers were slightly higher than that in TMAH developer, as shown in **Fig. 3-3(b).** For the 30% *t*-Boc PHS films, the peak impedance in the A-TMAH developers decreased from B-TMAH to P-TMAH, E-TMAH and TMAH in this sequence, as shown in **Figs. 3-2(d)** and **3-3(d)**. (For the 50-nm-thick films, the peak impedance in P-TMAH developer was approximately the same as that in the B-TMAH developer.)

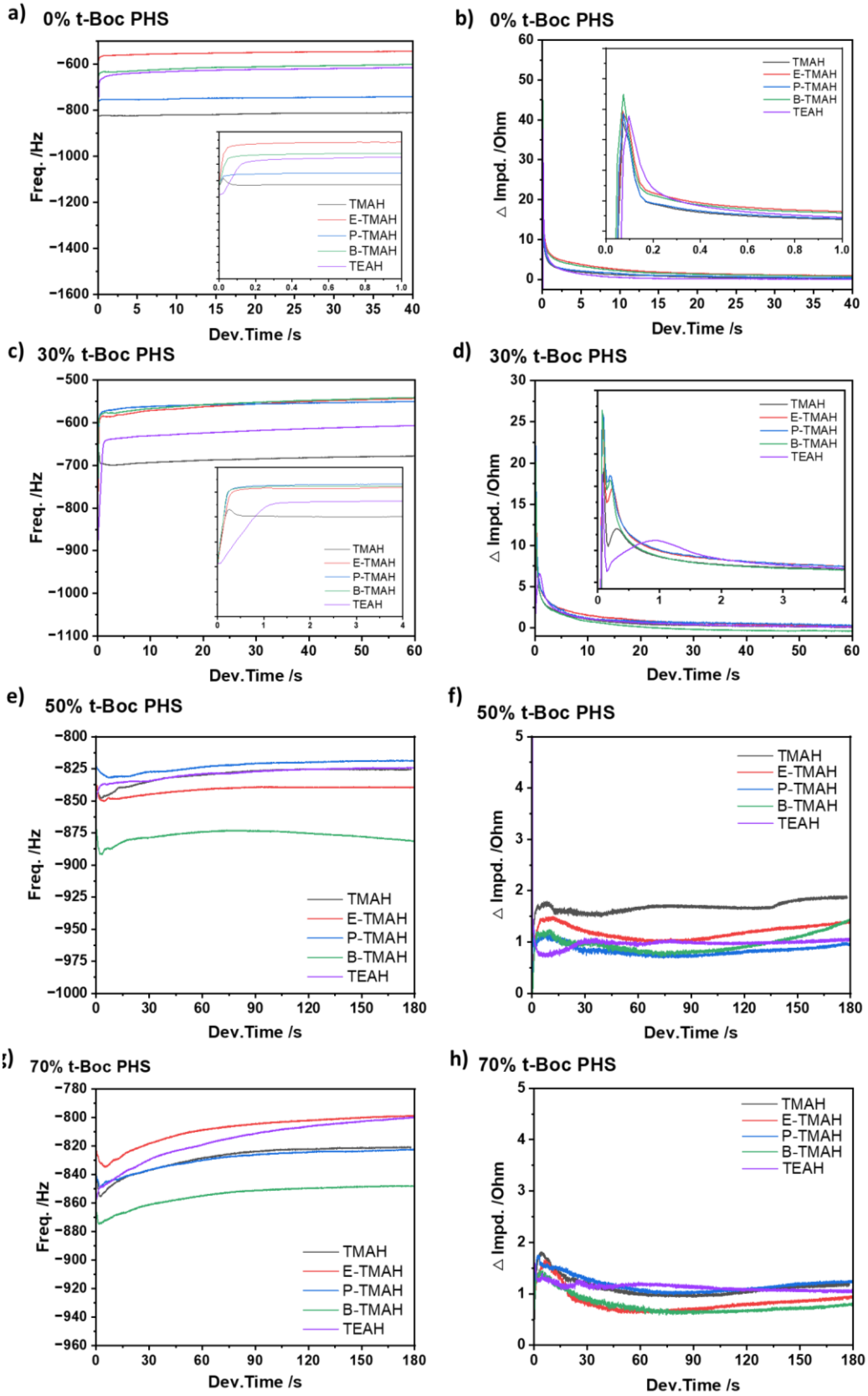

Fig. 3-2. Dissolution kinetics of *t*-Boc PHS films of 50 nm, as function of frequency and impedance variations. (a,b) 0%, (c,d) 30%, (e,f) 50%, and (g,h) 70% *t*-Boc PHS films.

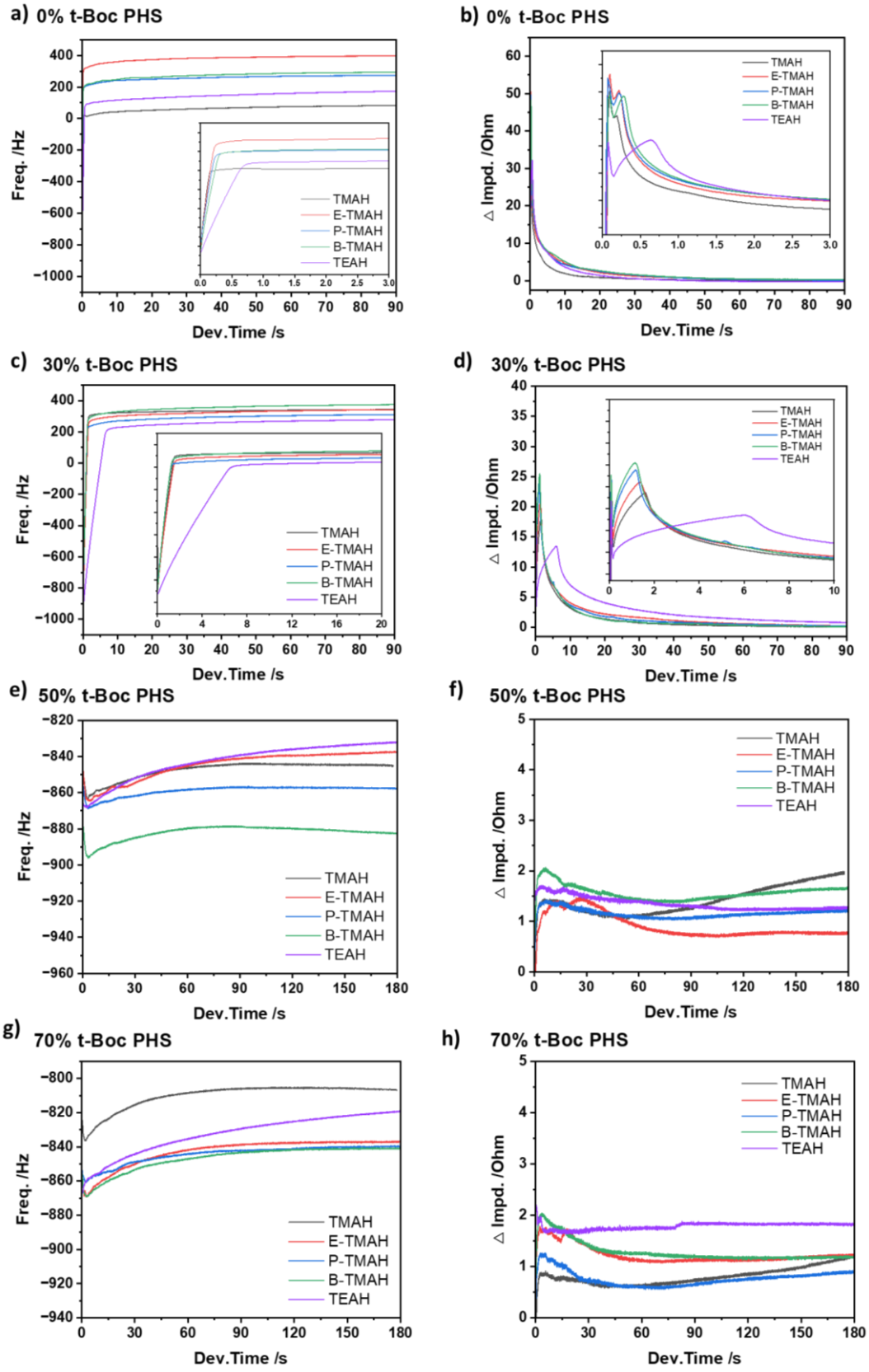

Fig. 3-3. Dissolution kinetics of *t*-Boc PHS films of 200 nm, as function of the frequency and impedance variations. (a,b) 0%, (c,d) 30%, (e,f) 50%, and (g,h) 70% *t*-Boc PHS films.

As discussed in **Sect. 3-2**, the impedance variation was related to the viscosity of the contacting layer. Simultaneously, two factors might affect solution viscosity namely: the concentration of the solute and the solvent itself.[31,32] In our study, the solvent is water, whereas the solutes are organic alkali (A-TMAH and TEAH) and *t*-Boc PHS. With the progress of dissolution, the dissolved polymer becomes abundant near the interface between the undissolved rigid film and the liquid phase, approaching the saturation state. To further elucidate the impacts of different developers and the solubility of *t*-Boc PHS on the impedance variation during the development, static measurement was applied instead of the time-dependent measurement of dissolution. In the static measurement, the developers and saturated solutions were directly dropped on the QCM substrate, and the impedance was measured by the analyzer.

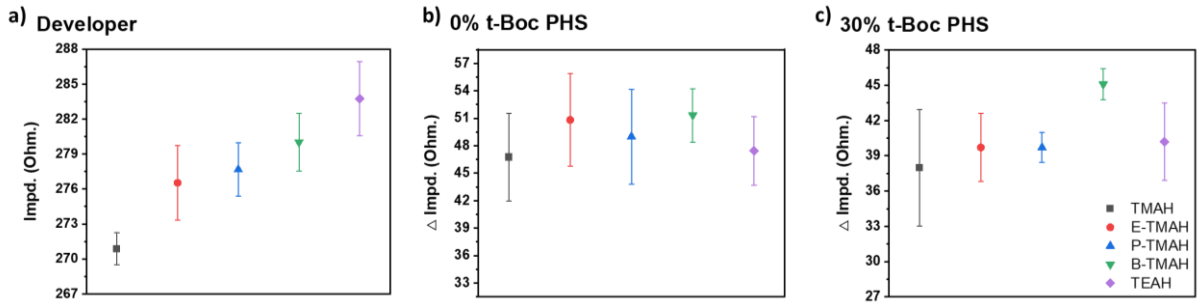

Fig. 3-4. (a) Impedances of pristine developers, (b) impedance changes of developers caused by the saturation of 0% *t*-Boc PHS, and (c) impedance changes of developers caused by the saturation of 30% *t*-Boc PHS. The baselines of impedance changes in (b) and (c) were the impedances of the corresponding pristine developers in (a).

As shown in **Fig. 3-4**, the static impedances of pristine developers and the impedance changes of the saturated developers with 0 and 30% *t*-Boc PHS were obtained. The impedance change baseline was set to the impedance of each pristine developer. For the pristine developers, the impedance was increased with the length of the alkyl chain of the alkyl trimethyl ammonium cation. This result indicates that the diffusion constant of polymer molecules decreases with the increase in the length of the alkyl chain. This is one of the reasons why the dissolution rate of 0% *t*-Boc PHS decreased with the increase in the length of the alkyl chain, as shown in **Figs. 3-3(a)** and **(b)**. However, the dissolution rate of 30% *t*-Boc PHS did not decrease despite the decrease of diffusion constant. The reason for this will be discussed later. For the 0%-*t*-Boc-PHS-saturated developers, the impedance changes of the developers due to the dissolved *t*-Boc PHS were

approximately the same. The impedance changes of the 30%-*t*-Boc-PHS-saturated developers were approximately the same except for that of the B-TMAH developer saturated with 30% *t*-Boc PHS. The impedance changes of the 30%-*t*-Boc-PHS-saturated developers were smaller than those of the 0%-*t*-Boc-PHS-saturated developers. Interestingly, the result of static measurement was not similar to that in the dynamic measurement, in which the impedance of TEAH was the lowest among the developers used. The maximum impedance changes attainable during the development of 200-nm-thick *t*-Boc PHS films **[Figs. 3-3(b)** and **(d)]** were smaller than the impedance changes of the corresponding saturated developers. This means that the developers near the dissolution front of *t*-Boc PHS films were not saturated with polymer molecules and the transient swelling layer formed during dissolution was thin in all the cases of 0 and 30% *t*-Boc PHS films.

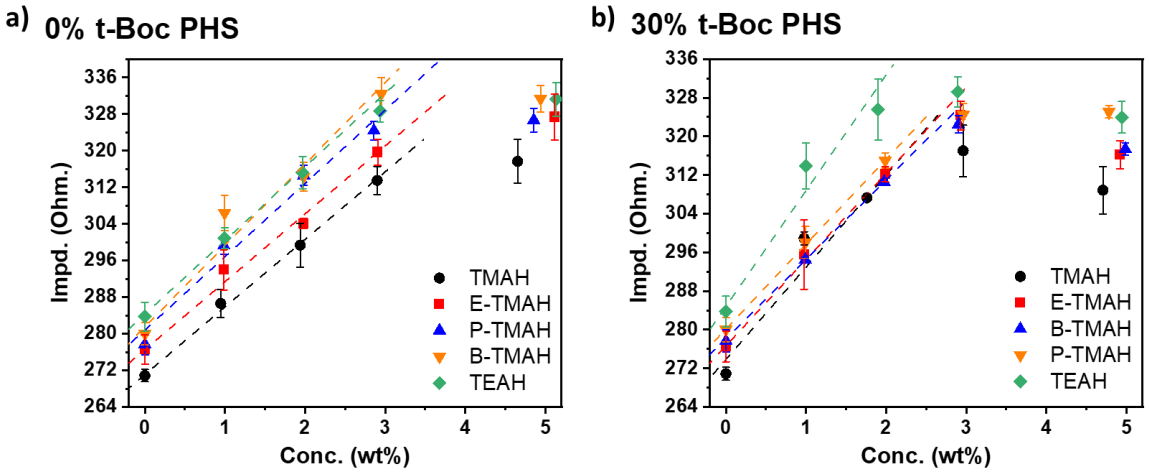

Fig. 3-5. Relationship between the impedance and concentration of (a) 0% *t*-Boc PHS and (b) 30% *t*-Boc PHS in A-TMAH and TEAH developers.

Figure 3-5 shows the impedances of developers with 1, 2, 3, and 5 wt% of 0 and 30% *t*-Boc PHS. The impedances of developers with 0 and 30% *t*-Boc PHS showed a linear relationship with the concentration of dissolved *t*-Boc PHS when their concentrations were low. The slopes for 0% *t*-Boc PHS solutions were approximately the same, whereas those for 30% *t*-Boc PHS solutions were different.

The solubility can be estimated from the impedance of the saturated developer and the dependence of the impedance on polymer concentration (the slopes of dashed lines shown in **Fig. 3-5**).[33] The estimated solubilities are listed in **Table 3-1** together with the impedances of pristine and saturated developers and the proportionality constants between *t*-Boc PHS concentration and

impedance change. The solubilities of 0% *t*-Boc PHS in the developers were approximately the same as the neutralization limitation of the developer at around 0.26 N. The solubility tended to decrease with the increase in the alkyl chain length of A-TMAH. For 30% *t*-Boc PHS, the solubility was lower than that of 0% *t*-Boc PHS. The solubility in TEAH was the lowest one among the developers, approximately 0.12 mol/L. Regarding the type of A-TMAH developer, E-, P-, and B-TMAH had higher solubilities, approximately 0.18 mol/L than TMAH (approximately 0.15 mol/L). This result was highly in accordance with the impedance variations observed during the development. The difference in the solubility of 30% *t*-Boc PHS in the developers showed an apparent correlation to its effect on the impedance during the development [**Figs. 3-2(d)** and **3-3(d)**]. On the other hand, the similar solubility of 0% *t*-Boc PHS showed a lower correlation, indicating that the impedance changes during the development [**Figs. 3-2(b)** and **3-3(b)**] were more likely affected by the dissolution process, as discussed previously, and/or the properties of films.

Table 3-1. Impedance, solubility, and proportionality constant between the impedance and concentration (slope) for 0 and 30% *t*-Boc PHS in A-TMAH and TEAH developers.

	Impedance			Solubility*				Slope	
	Pristine	0% *t*-Boc	30% *t*-Boc	0% *t*-Boc		30% *t*-Boc		0% *t*-Boc	30% *t*-Boc
	Ω	Ω	Ω	wt%	mol/L	wt%	mol/L	Ω/wt%	Ω/wt%
TMAH	270.9±1.4	317.7±4.8	308.9±5.0	3.2	0.27	2.3	0.15	14.8	19.1
E-TMAH	276.5±3.2	327.4±5.1	316.3±2.9	3.5	0.29	2.7	0.18	14.8	16.4
P-TMAH	277.7±2.3	326.7±5.2	317.4±1.3	2.8	0.23	2.7	0.18	16.0	17.6
B-TMAH	280.0±2.5	317.7±2.9	308.9±1.3	2.8	0.23	2.5	0.17	17.8	17.9
TEAH	283.8±3.2	327.4±3.7	316.3±3.3	2.8	0.23	1.8	0.12	16.1	24.0

*The solubility in wt% was obtained from the intersection point of the fitted curve shown in Fig. 5 with the impedance of the saturated developer; that in mol/L was calculated as: $Solubility_{(mol/L)} = Solubility_{(wt\%)} \times 10 / [(1-x) \times M_{PHS} + x \times M_{t\text{-}Boc\ PHS}]$, where $x=0.3$ or 0, $M_{PHS} = 120$ g/mol, and $M_{t\text{-}Boc\ PHS} = 220$ g/mol.

To obtain the diffusion ability of polymers in the developer, the DLS measurement was applied. The R_h and D of PHS and t-Boc PHS in A-TMAH and TEAH aqueous solution was shown in the **Table. 3-2**. As a consequence, the result was similar to that in the dissolution behaviors, while the impedance peak during the development was more related to the diffusion constant. Due to the high diffusion constant, the developer penetrates the polymer film more easily and rapidly dissolves the polymer, resulting in high viscosity on the film surface. More importantly, the

difference in dissolution behavior of PHS and *t*-Boc PHS could be quantitively described by the diffusion constant.

Table 3-2. The hydrodynamic radium (R_h) and diffusion constant (D) of *t*-Boc PHS in developers.

		0% t-Boc PHS		30% t-Boc PHS	
	η_s	R_h	D	R_h	D
	$mPa \cdot s$	nm	$10^{10}\, m^2 \cdot s^{-1}$	nm	$10^{10}\, m^2 \cdot s^{-1}$
TMAH	1.011	1.75	1.226	2.50	0.858
E-TMAH	1.057	1.9	1.080	2.23	0.912
P-TMAH	1.067	2.1	0.968	1.52	1.341
B-TMAH	1.086	2.05	0.975	1.50	1.332
TEAH	1.116	2.4	0.810	2.6	0.747

With the elongation of alkyl chains of the developer, its molecular size increased, inhibiting its penetration into the film. For the 0% t-Boc PHS, molecular size of the developer is considered as the cause for the dependence of the dissolution rate in A-TMAH developers, as well as the developer viscosity. However, the situation was completely different in the case of 30% *t*-Boc PHS, as discussed previously. Owing to the introduction of *t*-Boc groups in PHS, the dispersion (non-polar) component (one type of components in surface free energy) of PHS increased.[34] The elongation of one of the side chains is considered beneficial for the penetration of the developer into the film and the separation of nonpolar molecular interactions among 30% *t*-Boc PHS molecules.

Furthermore, the different dependences of dissolution kinetics of 0 and 30% *t*-Boc PHS films may lead to a potential improvement in actual development in lithography. After the light exposure, a gradient of protected unit concentration from the soluble to insoluble state is generated in the photoresist film.[4,35] The insoluble defects with high protected unit concentration tend to be stochastically generated near the resist side wall and substrate.[4,36] The property of A-TMAH with one long alkyl chain is expected to dissolve the region with high protected unit concentration and suppress the generation of such insoluble defects.

3-4. Conclusion

The QCM method was introduced in the research study of the dissolution kinetics and behaviors of PHS with different protection ratios of *t*-Boc groups in 0.26 N A-TMAH developers. The

dissolution kinetics in the E-, P-, and B-TMAH aqueous developers were compared with those of the TMAH and TEAH aqueous solutions. The *t*-Boc PHS films with the protection ratios of 0 and 30% were soluble in developers, whereas those with protection ratios of 50 and 70% *t*-Boc PHS films were insoluble. The order of dissolution rates of 0 and 30% *t*-Boc PHS was as follows: for 0% *t*-Boc PHS, TMAH＞E-TMAH＞P-TMAH＞B-TMAH＞TEAH, whereas for 30% *t*-Boc PHS, E-TMAH ＞ P-TMAH ＞ B-TMAH ＞ TMAH ＞ TEAH. Similar results were achieved in the hydrodynamic radius (R_h) and diffusion constant (D) by the DLS measurement. Such differences in dissolution rate and diffusion constant indicates that the elongation of one of the alkyl chains of the tetramethylammonium cation is beneficial for the penetration of the developer and the separation of non-polar molecular interactions among 30% *t*-Boc PHS molecules.

References

1) T. Itani, P. A. Gargini, P. P. Naulleau, and K. G. Ronse, Proc. SPIE **11147**, 1114701 (2019).

2) T. Kozawa, J. J. Santillan, and T. Itani, Jpn. J. Appl. Phys. **52**, 076502 (2013).

3) H. J. Levinson, Jpn. J. Appl. Phys. **61**, SD0803 (2022).

4) T. Kozawa, Jpn. J. Appl. Phys. **61**, 106502 (2022).

5) S. Nagahara, C. Q. Dinh, K. Yoshida, G. Shiraishi, Y. Kondo, K. Yoshihara, K. Nafus, J. S. Petersen, D. De Simone, P. Foubert, G. Vandenberghe, H.-J. Stock, and B. Meliorisz, Proc. SPIE **11326**, 113260A (2020).

6) E. Buitrago, S. Nagahara, O. Yildirim, H. Nakagawa, S. Tagawa, M. Meeuwissen, T. Nagai, T. Naruoka, C. Verspaget, R. Hoefnagels, G. Rispens, G. Shiraishi, Y. Terashita, Y. Minekawa, K. Yoshihara, A. Oshima, M. Vockenhuber, and Y. Ekinci, J. Micro/Nanolithography, MEMS, and MOEMS **15**, 033502 (2016).

7) I. Mochi, K. Garrido Olvera, M. Meeuwissen, O. Yildirim, R. Custers, R. Hoefnagels, G. Rispens, M. Vockenhuber, Y. Ekinci, and Z. Tasdemir, Proc. SPIE **10583**, 105831W (2018).

8) K. Kasahara, H. Xu, V. Kosma, J. Odent, E. P. Giannelis, and C. K. Ober, J. Photopolym. Sci. Technol. **30**, 93 (2017).

9) J. Hotalen, M. Murphy, W. Earley, M. Vockenhuber, Y. Ekinci, D. A. Freedman, and R. L. Brainard, Proc. SPIE **10143**, 1014309 (2017).

10) S. Takechi, A. Kotachi, M. Takahashi, and I. Hanyu, Proc. SPIE **3049**, 519 (1997).

11) T. Itani and J. J. Santillan, J. Vac. Sci. Technol. B **27**, 2986 (2009).

12) M. Harumoto, J. J. Santillan, T. Itani, and T. Kozawa, Jpn. J. Appl. Phys. 61, 056506 (2022).
13) M. Harumoto, A. F. Santos, J. J. Santillan, T. Itani, and T. Kozawa, Jpn. J. Appl. Phys. **62**, 016503 (2023).
14) M. Harumoto, A. F. Santos, J. J. Santillan, T. Itani, and T. Kozawa, Jpn. J. Appl. Phys. **62**, SG1037 (2023).
15) Y. T. Ito, H. Betsumiya, T. Kozawa, K. Sakamoto, and M. Muramatsu, Jpn. J. Appl. Phys. **61**, 066506 (2022).
16) H. Betsumiya, Y. T. Ito, T. Kozawa, K. Sakamoto, and M. Muramatsu, Jpn. J. Appl. Phys. **62**, 036503 (2023).
17) J. J. Santillan, M. Harumoto, T. Motono, A. F. Santos, C. Mori, Y. Tanaka, H. Stokes, M. Asai, and T. Itani, Jpn. J. Appl. Phys. **60**, SCCC01 (2021).
18) J. J. Santillan, K. Shimizu, R. Otogawa, and T. Itani, J. Photopolym. Sci. Technol. **35**, 67 (2022).
19) A. Sekiguchi, J. Photopolym. Sci. Technol. **23**, 421 (2010).
20) M. Toriumi, Proc. SPIE **7273**, 72732Y (2009).
21) S. W. Lee, W. D. Hinsberg, and K. K. Kanazawa, Anal. Chem. **74**, 125 (2002).
22) K. K. Kanazawa, Faraday Discuss. **107**, 77 (1997).
23) G. Sauerbrey, Z. Phys. **155**, 206 (1959).
24) K. K. Kanazawa and J. G. Gordon, Anal. Chem. **57**, 1770 (1985).
25) M. V. Voinova, M. Rodahl, M. Jonson, and B. Kasemo, Phys. Scr. **59**, 391 (1999).
26) S. J. Martin, V. E. Granstaff, and G. C. Frye, Anal. Chem. **63**, 2272 (1991).
27) N. Tanaka, K. Matsuoka, T. Kozawa, T. Ikeda, Y. Komuro, and D. Kawana, Jpn. J. Appl. Phys. **61**, SD1016 (2022).
28) W. Hinsberg, F. A. Houle, S. W. Lee, H. Ito, and K. Kanazawa, Macromolecules **38**, 1882 (2005).
29) W. Hinsberg, S.-W. Lee, H. Ito, D. Hornea, and K. Kanazawa, Proc. SPIE **4345**, 1 (2001).
30) Y. Iwashige, Y. T. Ito, T. Kozawa, K. Sakamoto, and M. Muramatsu, Jpn. J. Appl. Phys. **62**, 036502 (2023).
31) T. F. Ford, J. Phys. Chem. **64**, 1168 (1960).
32) S. Fendt, S. Padmanabhan, H. W. Blanch, and J. M. Prausnitz, J. Chem. Eng. Data. **56**, 31

(2011).
33) Y. T. Ito, K. Watanabe, Y. Jin, T. Kozawa, K. Sakamoto, and M. Muramatsu, Jpn. J. Appl. Phys. **63**, 018002 (2024).
34) H. Betsumiya, Y. Jin, Y. T. Ito, T. Kozawa, K. Sakamoto, and M. Muramatsu, Jpn. J. Appl. Phys. **62**, 066501 (2023).
35) T. Kozawa, Jpn. J. Appl. Phys. **62**, 016509 (2023).
36) T. Kozawa, Jpn. J. Appl. Phys. **62**, 076501 (2023).

Summary

In chapter 1, the relationship between the attenuation rate (α) of photoresist film during the development and the surface free energy (SFE) of underlayer was revealed. For the materials, the poly(4-hydroxystyrene) partially protected by tert-butoxycarbonyl (t-Boc) group with 0, 10 and 30% was used as the photoresist. The surface free energy (SFE) of underlayer was varied. The tetramethylammonium hydroxide (TMAH) aqueous solution was used as the developer and concentration was 2.38, 1.43 and 0.95 wt%. For the experiment, dissolution kinetics during the development was detected by quartz crystal microbalance (QCM) method. The α, a factor related to the diffusion process of dissolved polymer in the developer, was obtained by the curve fitting of impedance variation, followed by the equation: $Z = \frac{z_0}{(t-t_0)^{\alpha}} + b$. In this study, the SFE ratio, the ratio of polar to dispersion component, was introduced to connect the relationship with α. As a result, an obvious tendency was observed between α and SFE ratio. With the increased SFE ratio of underlayer, the α was first descended and increased. In addition, an inflection point existed in the tendency. The inflection points with the lowest α, indicated the strongest interaction between the underlayer and photoresist films. The position of α would right shift with the decrease in developer concentration and increase of protection ratio of t-Boc PHS. It should be noticed the behavior of underlayer with halogen groups showed abnormal performance. The reason was speculated to the influence on halogen bonding existed between the underlayer and resist polymer.

In chapter 2, the influence of underlayer on the deprotection reaction of photoresist film with three components, t-Boc PHS/TPS-nf/TPS-sal was revealed, as well as their dissolution kinetics in the TMAH aqueous solution. The dissolution kinetics was revealed by the QCM method. The underlayer had a complicated effect on the photoresist during dissolution. In particular, the underlayer significantly affected the formation of the transient swelling layer and dissolution kinetics at an exposure dose close to the photoresist sensitivity, namely, at the critical exposure dose for solubilizing the photoresist films. For the photoresist used in this study, the dissolution kinetics was strongly (negatively from the viewpoint of photoresist performance) affected by the underlayers at an SFE ratio of 0.26–0.28. The results obtained in this chapter suggested that the adjustment of the polar and non-polar components of the SFE of the underlayers was required in accordance with the chemical conditions of photoresist films at an exposure dose close to the photoresist sensitivity for the precise control of dissolution kinetics, namely, the pattern shape. Furthermore, the proton affinity of the end groups of the underlayers probably affected the progress of the acid-catalytic reaction, and thereby, the dissolution kinetics.

In chapter 3, the dissolution kinetics of photoresist film of *t*-Boc PHS with different protection ratio in the novel developers, alkyl-trimethyl-ammonium hydroxide (A-TMAH) aqueous solution, was revealed. The QCM method was introduced in the research study of the dissolution kinetics. As a result, dissolution kinetics in the E-, P-, and B-TMAH aqueous developers were compared with those of the TMAH and TEAH aqueous solutions. The *t*-Boc PHS films with the protection ratios of 0 and 30% were soluble in developers, whereas those with protection ratios of 50 and 70% *t*-Boc PHS films were insoluble. The order of dissolution rates of 0 and 30% *t*-Boc PHS was as follows: for 0% *t*-Boc PHS, TMAH＞E-TMAH＞P-TMAH＞B-TMAH＞TEAH, whereas for 30% *t*-Boc PHS, E-TMAH＞P-TMAH＞B-TMAH＞TMAH＞TEAH. Similar results were obtained in the hydrodynamic radius (R_h) and diffusion constant (D) by the DLS measurement. Such differences in dissolution rate and diffusion constant indicates that the elongation of one of the alkyl chains of the tetramethylammonium cation is beneficial for the penetration of the developer and the separation of non-polar molecular interactions among 30% *t*-Boc PHS molecules.

As a summary, this study revealed the relationship between the underlayer and photoresist film in terms of the surface free energy. The effective factor of SFE was neither polar nor dispersion component, but the SFE ratio, the polar to dispersion component. In addition, the dissolution kinetics of resist film changing with the deprotection progress was revealed. This result was meaningful in real lithography. It could elucidate the reason for pattern defects in the insufficient reaction progress to some degree. The novel developers, the alternative of TMAH, had an interesting result in the dissolution kinetics of *t*-Boc PHS. An obvious contrast in dissolution rate of resist film and diffusion constant of dissolved polymer was suggestive to the development in the real lithography as well. Such contrast could probably restrain the pattern defect, such as the bridging due to the threshold of protection ratio in the resist film, resulting in a broader dimension window. The research in this thesis was believed to give a step or guidance to real lithography in manufacturing.

List of Publications

1. Dissolution dynamics of poly(4-hydroxystyrene) partially protected with t-butoxycarbonyl group in alkyltrimethylammonium hydroxide aqueous developers,

Jiahao Wang and Takahiro Kozawa,

Jpn. J. Appl. Phys. **63**, 076503 (2024)

DOI: 10.35848/1347-4065/ad5e26

2. Relationship between the surface free energy of underlayers and the dissolution kinetics of poly(4-hydroxystyrene) partially protected by t-butoxycarbonyl groups in tetramethylammonium hydroxide aqueous developer,

Jiahao Wang and Takahiro Kozawa,

Jpn. J. Appl. Phys. **63**, 096502 (2024)

DOI: 10.35848/1347-4065/ad6f86

3. Influence of underlayer on development of chemically amplified photoresist film in tetramethylammonium hydroxide (TMAH) aqueous developer,

Jiahao Wang and Takahiro KOZAWA,

Jpn. J. Appl. Phys. **64**, 036502 (2025)

DOI: 10.35848/1347-4065/adb5e2

Acknowledgements

This study was proceeded with the guidance of Prof. Takahiro Kozawa at the Department of Beam Material Science, SANKEN, Osaka University. I would like to express my sincere appreciation for his kind support, constructive suggestions and gentle encouragement during the work.

I'm grateful to Prof. Ken-ichi Nakayama and Prof. Hiroshi Uyama, at the Division of Applied Chemistry, Graduate School of Engineering in Osaka University, for reviewing this thesis and giving their comments and suggestions.

I would like to express my appreciation to the staff members of Kozawa Lab., Assoc. Prof. Yusa Muroya, Asst. Prof. Kazumasa Okamoto, Mr. Akihiro Konda, Ms. Kyoko Watanabe, Ms. Mikiko Kozawa, Ms. Kinuko Watanabe, Ms. Yuki Ishimaru, Ms. Yukiko Sasaki, Ms. Kyoko Matsuoka, and Ms. Arisa Matsuo to support my research. My spirits were obtained through the discussions and comments in these years.

I would like to thank the students of Kozawa Lab; Ms. Takata, Ms. Betsumiya, Ms. Jin, Mr. Iwashige, Ms. Tsuda, Mr. Nishimoto, Mr. Kaneba, Mr. Hashimoto, Mr. Fuku, and Mr. Masuda. My motivation and passion remained and never faded through their discussion, questioning and recognition during the daily laboratory life. I hope their life is full of success and happiness in the futre.

Finally, I would like to express my gratitude to my parents as well for their understanding, encouragement, and altruistic support.

The underlayer utilized in this research was supported by Nissan Chemical Corp. and parts of the developer were provided by Tokuyama Corp.